

# The Existence and Stability of Spike Equilibria in the One-Dimensional Gray-Scott Model: The Low Feed-Rate Regime

Theodore Kolokolnikov\*, Michael J. Ward†, Juncheng Wei‡

## Abstract

In a singularly perturbed limit of small diffusivity  $\varepsilon$  of one of the two chemical species, equilibrium spike solutions to the Gray-Scott model on a bounded one-dimensional domain are constructed asymptotically using the method of matched asymptotic expansions. The equilibria that are constructed are symmetric  $k$ -spike patterns where the spikes have equal heights. Two distinguished limits in terms of a dimensionless parameter in the reaction-diffusion system are considered: the low feed-rate regime and the intermediate regime. In the low feed-rate regime, the solution branches of  $k$ -spike equilibria are found to have a saddle-node bifurcation structure. The stability properties of these branches of solutions are analyzed with respect to the large eigenvalues  $\lambda$  in the spectrum of the linearization. These eigenvalues, which have the property that  $\lambda = O(1)$  as  $\varepsilon \rightarrow 0$ , govern the stability of the solution on an  $O(1)$  time-scale. Precise conditions, in terms of the non-dimensional parameters, for the stability of symmetric  $k$ -spike equilibrium solutions with respect to this class of eigenvalues are obtained. In the low feed-rate regime, it is shown that a large eigenvalue instability leads either to a competition instability, whereby certain spikes in a sequence are annihilated, or an oscillatory instability (typically synchronous) of the spike amplitudes as a result of a Hopf bifurcation. In the intermediate regime, it is shown that only oscillatory instabilities are possible, and a scaling-law determining the onset of such instabilities is derived. Detailed numerical simulations are performed to confirm the results of the stability theory. It is also shown that there is an equivalence principle between spectral properties of the Gray-Scott model in the low feed-rate regime and the Gierer-Meinhardt model of morphogenesis. Finally, our results are compared with previous analytical work on the Gray-Scott model.

## 1 Introduction

We study the existence and stability of equilibrium spike patterns in the one-dimensional Gray-Scott (GS) model in a particular parameter regime. The GS model, introduced for continuously stirred systems in [10], models an irreversible reaction involving two reactants in a gel reactor, where the reactor is maintained in contact with a reservoir of one of the two chemical species. In nondimensional variables, this system is

$$V_T = D_v V_{XX} - (F + k)V + UV^2, \quad 0 < X < L, \quad T > 0; \quad V_X = 0, \quad X = 0, L, \quad (1.1a)$$

$$U_T = D_u U_{XX} + F(1 - U) - UV^2, \quad 0 < X < L, \quad T > 0; \quad U_X = 0, \quad X = 0, L. \quad (1.1b)$$

Here  $D_u > 0$ ,  $D_v > 0$  are the constant diffusivities,  $F > 0$  is the feed rate, and  $k > 0$  is a reaction-time constant. For various ranges of these parameters, (1.1) and its two-dimensional counterpart, are known

---

\*Department of Mathematics, University of British Columbia, Vancouver, Canada V6T 1Z2

†Department of Mathematics, University of British Columbia, Vancouver, Canada V6T 1Z2, (corresponding author)

‡Department of Mathematics, Chinese University of Hong Kong, New Territories, Hong Kong

to possess a rich solution structure including the existence of stable standing pulses, the propagation of traveling waves, pulse-replication behavior, and spatio-temporal chaos (cf. [4]–[7], [8], [15], [16], [19], [20], [24], [25], [26], [28], [30], [31], [32], [33], [34], [35], and [38]).

We will analyze (1.1) in the singularly perturbed limit where  $D_v/D_u$  is asymptotically small. In our formulation, it is convenient to introduce the change of variables  $v = V/\sqrt{F}$ ,  $x = -1 + 2X/L$ , and  $t = (F + k)T$  as was used in [26]. This leads to the alternative dimensionless system

$$v_t = \varepsilon^2 v_{xx} - v + Auv^2, \quad -1 < x < 1, \quad t > 0; \quad v_x(\pm 1, t) = 0, \quad (1.2a)$$

$$\tau u_t = Du_{xx} + (1 - u) - uv^2 \quad -1 < x < 1, \quad t > 0; \quad u_x(\pm 1, t) = 0. \quad (1.2b)$$

Here  $A > 0$ ,  $D > 0$ ,  $\tau > 1$ , and  $0 < \varepsilon \ll 1$ , are defined in terms of  $D_u$ ,  $D_v$ ,  $L$ ,  $F$ , and  $k$ , by

$$D \equiv \frac{4D_u}{FL^2}, \quad \varepsilon^2 \equiv \frac{4D_v}{L^2(F + k)}, \quad \tau \equiv \frac{F + k}{F}, \quad A \equiv \frac{\sqrt{F}}{F + k}. \quad (1.3)$$

The system (1.2) is particularly convenient in that it shows that the construction of equilibrium solutions depends only on the parameters  $A$  and  $D$ , while the parameter  $\tau > 1$  only influences the stability of these solutions. The influence of the finite domain and the strength of the inter-spike interactions depends on  $D$ . For a  $k$ -spike solution, the finite domain and the inter-spike interactions are significant only when  $k\sqrt{D} = O(1)$ . When  $k\sqrt{D} \ll 1$ , an equilibrium  $k$ -spike solution for (1.2) is composed, essentially, of  $k$  identical copies of a one-spike solution for the infinite-line problem, where (1.2) is defined on  $-\infty < x < \infty$ .

We will analyze the existence and stability of equilibrium  $k$ -spike solutions for (1.2) in the limit  $\varepsilon \rightarrow 0$  and for  $D = O(1)$ . There are three regimes for  $A$  where different behaviors are obtained. For the low feed-rate regime  $A = O(\varepsilon^{1/2})$  there is a saddle-node bifurcation structure of equilibrium  $k$ -spike solutions, and we find that the stability of these solutions depends intricately on  $A$ ,  $D$ , and  $\tau$ . For the intermediate regime  $O(\varepsilon^{1/2}) \ll A \ll O(1)$  there are certain scaling laws in terms of a universal nonlocal eigenvalue problem that determine the stability of equilibrium spike solutions. Finally, in the high feed-rate regime  $A = O(1)$  the equilibrium spike solutions again exhibit a saddle-node bifurcation structure, and this regime is intimately connected with a pulse-splitting behavior of spike patterns. In this regime, which is studied in the companion paper [17], the effect of the finite domain is crucial in the analysis.

We now summarize our results for the low feed-rate regime. In this regime, we introduce  $\mathcal{A}$  and  $\nu$  by

$$A = \varepsilon^{1/2} \mathcal{A}, \quad v = \varepsilon^{-1/2} \nu. \quad (1.4)$$

In terms of (1.4), (1.2) is transformed to

$$\nu_t = \varepsilon^2 \nu_{xx} - \nu + \mathcal{A} \nu^2, \quad -1 < x < 1, \quad t > 0; \quad \nu_x(\pm 1, t) = 0, \quad (1.5a)$$

$$\tau u_t = Du_{xx} + (1 - u) - \varepsilon^{-1} u \nu^2 \quad -1 < x < 1, \quad t > 0; \quad u_x(\pm 1, t) = 0. \quad (1.5b)$$

For  $\varepsilon \ll 1$ , in §2 we construct  $k$ -spike equilibrium solutions where the spikes in  $\nu$  have a common amplitude. For these symmetric  $k$ -spike equilibria, we show that for each  $k = 1, 2, \dots$  there are two branches of such solutions for (1.5) when  $\mathcal{A} > \mathcal{A}_{ke}$ . These branches are parametrized in terms of a parameter  $s$  by

$$\mathcal{A} = \mathcal{A}_{ke} \frac{(1 + s)}{2\sqrt{s}}, \quad 0 < s < \infty; \quad \mathcal{A}_{ke} \equiv \sqrt{\frac{12\theta_0}{\tanh(\theta_0/k)}}, \quad \theta_0 \equiv D^{-1/2}, \quad U_{\pm} = \frac{1}{s + 1}. \quad (1.6)$$

Here  $U_{\pm} \sim u(x_j)$ , where  $x_j$  is a spike location. For  $D = 0.75$ , in Fig. 1 we plot the  $L_2$  norm of  $\nu$  versus  $\mathcal{A}$  for the  $k$ -spike solution branches for  $k = 1, \dots, 4$  showing the existence thresholds  $\mathcal{A}_{ke}$  (see (2.11) below for the definition of the norm). For each  $k$ , the upper branch in this figure, where  $s > 1$ , is referred to as the large solution branch, while the lower branch, where  $0 < s < 1$ , is called the small solution branch.

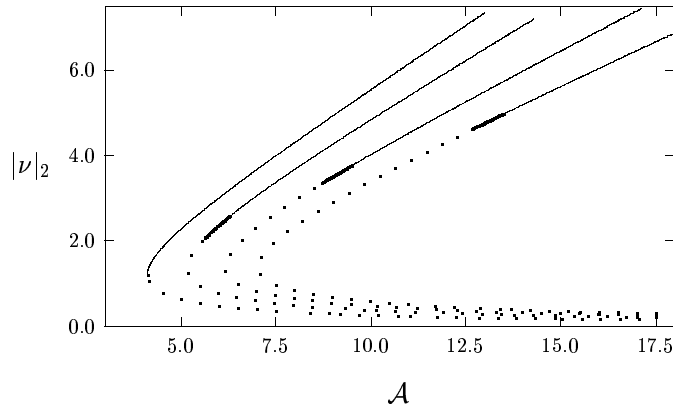


Figure 1:  $|\nu|_2$  versus  $\mathcal{A}$  for  $D = 0.75$  and  $k = 1, \dots, 4$ . The dashed lines are unstable for  $\tau \geq 0$ . The heavy solid lines are stable only with respect to the large eigenvalues when  $\tau < \tau_{hL}$ . The solid lines are stable with respect to both the large and small eigenvalues when  $\tau < \tau_{hL}$ . The fold values  $\mathcal{A}_{ke}$  increase with  $k$ , and  $\mathcal{A}_{kL}$  corresponds to where the dashed and heavy solid lines intersect (for  $k = 1$ ,  $\mathcal{A}_{kL} = \mathcal{A}_{ke}$ ).

In §3 we formally derive a nonlocal eigenvalue problem (NLEP) governing the stability of the symmetric  $k$ -spike equilibrium solutions constructed in §2 with respect to the eigenvalues of order  $O(1)$  in the spectrum of the linearization. These eigenvalues, referred to as the large eigenvalues, are associated with the initiation of profile instabilities, whereby the spike amplitudes will either oscillate, typically with a common frequency and phase, or else undergo a competition instability leading to the monotonic annihilation of spikes in a spike sequence. From this NLEP, we prove in Proposition 3.10 that the small solution branch is unconditionally unstable for any  $\tau > 0$  and  $D > 0$ . The stability properties of the large solution branch is significantly more intricate. In particular, for each  $k = 1, 2, \dots$  and  $D > 0$  fixed, we prove that there exists a threshold value  $\mathcal{A}_{kL}$ , with  $\mathcal{A}_{kL} > \mathcal{A}_{ke}$ , such that the large solution branch is stable with respect to profile instabilities for  $\mathcal{A} > \mathcal{A}_{kL}$  when  $\tau < \tau_{hL}$ . An explicit formula for  $\mathcal{A}_{kL}$  is given below in (3.25b). For the range  $\mathcal{A} > \mathcal{A}_{kL}$ , there is a Hopf bifurcation as  $\tau$  exceeds some critical value  $\tau_{hL}$ . This bifurcation typically leads to a synchronous oscillatory instability in the spike amplitudes. The precise results are given below in Propositions 3.11, 3.13, and 3.15. On the range  $\mathcal{A}_{ke} < \mathcal{A} < \mathcal{A}_{kL}$  for the large solution branch, the spectrum of the linearization of (1.5) around a symmetric  $k$ -spike equilibrium solution contains at least one (unstable) real and positive eigenvalue. The existence of such eigenvalues in this parameter range is the mechanism for the initiation of competition instabilities whereby certain spikes in a spike sequence are annihilated. Precise spectral results for this range of  $\mathcal{A}$  are given below in Proposition 3.12. The critical values  $\mathcal{A}_{kL}$  for  $k = 2, 3, 4$  and  $D = 0.75$  can be seen in Fig. 1.

We now illustrate these instabilities for (1.5) for the parameter set  $k = 4$ ,  $D = 0.1$ , and  $\varepsilon = 0.01$  (this is

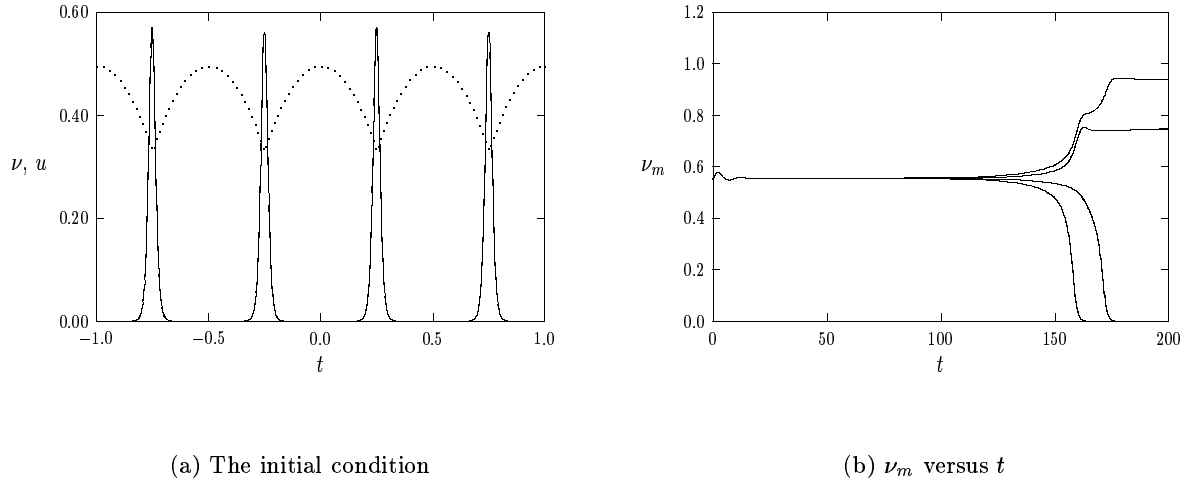


Figure 2: The parameters are  $k = 4$ ,  $D = 0.1$ ,  $\mathcal{A} = 8.0$ ,  $\varepsilon = 0.01$ , and  $\tau = 2$ . Left figure: the initial condition for  $\nu$  (solid curve) and  $u$  (dashed curve). Right figure: The spike amplitudes  $\nu_m$ . The second and fourth spikes are annihilated by a spike competition. Of the two remaining spikes, the third spike has the larger amplitude.

Example 3 of §3.3). For this example, our theory yields  $\mathcal{A}_{kL} = 8.127$ . For the value  $\mathcal{A} = 8.0$ , in Fig. 2(a) we show a 1% perturbation in the equilibrium solution, which we use as the initial condition for (1.5). Since  $\mathcal{A} < \mathcal{A}_{kL}$ , our theory predicts the initiation of a spike competition process. In Fig. 2(b) we plot the spike amplitudes, defined as the values of  $\nu$  at its local maxima, versus time showing a spike competition process leading to the annihilation of two spikes. In Fig. 3(a) where  $\mathcal{A} = 8.302 > \mathcal{A}_{kL}$  we show a synchronous decaying oscillation in the spike amplitudes when  $\tau = 3.8$ . In Fig. 3(b), where  $\tau = 4.1$  exceeds the Hopf bifurcation value, we show a synchronous oscillatory instability leading to the simultaneous collapse of the four spikes. A theoretical analysis of the initiation of these fast instabilities is given in §3. Competition and synchronous oscillatory instabilities in the low feed-rate regime, which occur as a result of the finite domain and a strong inter-spike coupling, have not been previously reported for the GS model (1.5).

The *intermediate regime*, defined by  $O(1) \ll \mathcal{A} \ll O(\varepsilon^{-1/2})$ , is analyzed in §4. In this regime, there are no competition instabilities for spikes separated by  $O(1)$  distances. In this regime, we show that such instabilities can only occur if the inter-spike separation distance  $L$  satisfies  $L < L_m \sim (12\gamma_k D \varepsilon A^{-2})^{1/3} \ll 1$ , where  $A = \varepsilon^{1/2} \mathcal{A}$  and  $\gamma_k = 1 + \cos(\pi/k)$ . In Principal Result 4.2 we derive a universal nonlocal eigenvalue problem, independent of  $D$  and  $k$ , that governs the stability of a symmetric  $k$ -spike equilibrium solution with respect to oscillatory instabilities. In terms of a critical value of this eigenvalue problem, in Proposition 4.3 we derive a scaling law for the Hopf bifurcation value of  $\tau$ . In the intermediate regime the Hopf bifurcation value is  $\tau = O(\mathcal{A}^4)$ . Thus, there are no oscillatory instabilities when  $\tau = O(1)$ .

Although it is difficult to translate detailed spectral results into precise physical mechanisms for instability, a qualitative mechanism for the two types of instabilities is as follows. For a given value of  $\mathcal{A}$  and for a fixed small value of  $\tau$ , a competition instability occurs when either  $D$  is too large, or equivalently

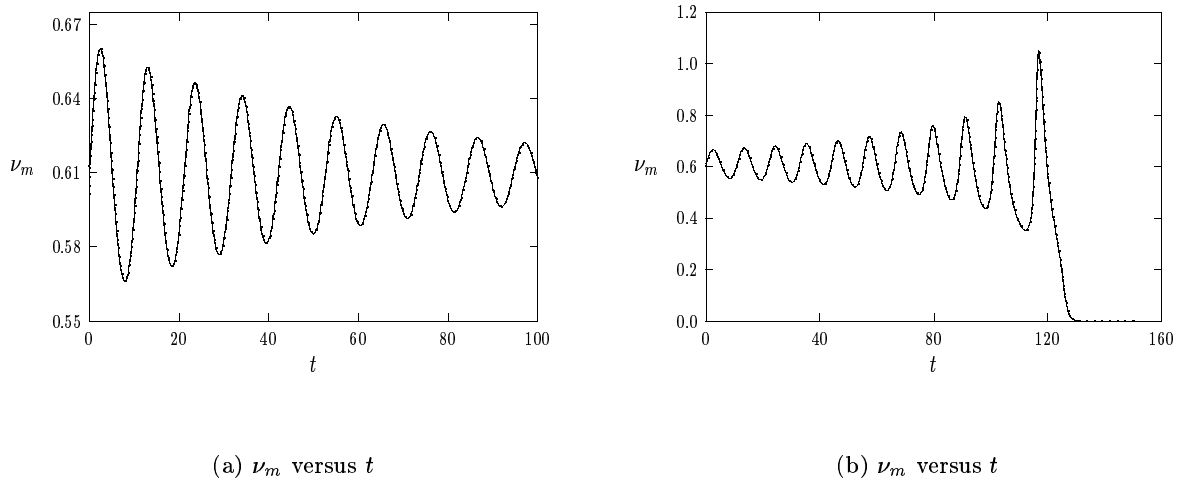


Figure 3: Spike amplitudes for  $k = 4$ ,  $D = 0.1$ ,  $\mathcal{A} = 8.302$ , and  $\varepsilon = 0.01$ . Left figure: synchronous decaying oscillation in the amplitudes for  $\tau = 3.8$ . Bottom right: synchronous oscillatory instability for  $\tau = 4.1$ , leading to simultaneous annihilation. The spike amplitudes trace out identical trajectories.

when the spikes are too close together. For  $D$  large, the inhibitor  $u$  diffuses over a large spatial extent thereby preventing the occurrence of another spike. This instability is probably a counterpart of the spike *over-crowding* instability observed numerically in the weak-interaction regime for the two-dimensional GS model in [32], and observed experimentally in [19] in the ferrocyanide-iodate-sulphite reaction. For  $D$  sufficiently large and  $\tau$  small, there are  $k - 1$  positive real eigenvalues in the spectrum of the linearization. The positive real eigenvalue responsible for a competition instability is the last real eigenvalue that remains in the right half-plane as  $D$  is decreased. Alternatively, for a fixed  $D$ , oscillatory instabilities occur when  $\tau$  is sufficiently large. For  $\tau$  large, the inhibitor field  $u$  responds sluggishly to small temporal changes in the spike pattern. This leads to an oscillatory feedback loop typical in delay-type differential equations.

Similar types of competition and synchronous oscillatory instabilities of equilibrium spike solutions have been analyzed in [39] for the Gierer-Meinhardt (GM) model of morphogenesis introduced in [9], and used to model localization problems in biological pattern formation and sea-shell patterns (cf. [11], [22], [23]). In dimensionless form, this system can be written as

$$a_t = \varepsilon^2 a_{xx} - a + \frac{a^p}{h^q}, \quad \tau h_t = D h_{xx} - h + \varepsilon^{-1} \frac{a^m}{h^s}, \quad -1 < x < 1, \quad t > 0, \quad (1.7)$$

with  $a_x = h_x$  at  $x = \pm 1$ . Here  $a$  and  $h$  are the activator and inhibitor fields, with  $0 < \varepsilon^2 \ll 1$ ,  $D > 0$ , and  $\tau \geq 0$ . The usual assumption on the GM exponents  $(p, q, m, s)$  (cf. [9]) are that they satisfy

$$p > 1, \quad q > 0, \quad m > 1, \quad s \geq 0, \quad \text{with} \quad \zeta \equiv \frac{qm}{(p-1)} - (s+1) > 0. \quad (1.8)$$

The relationship between oscillatory and competition instabilities in the GS and GM models is made precise in Proposition 3.3 below where we show that the nonlocal eigenvalue problem for instabilities in the GS

model in the low feed-rate regime is identical to the nonlocal eigenvalue problem for the GM model with exponent set  $(p, q, m, s) = (2, s, 2, s)$ , where  $s$  is defined in (1.6). This spectral equivalence principle is a new result, and it allows us to use many of the detailed spectral results derived in [39] for the GM model.

More generally, instabilities of spike patterns as a result of positive real eigenvalues, leading to spike annihilation, have been studied in other systems. In particular, for scalar nonlocal singularly perturbed parabolic equations where the steady-state problem has a homoclinic connection, a  $k$ -spike pattern for  $k > 1$  is unstable as a result of  $k - 1$  positive real eigenvalues (see Remark 3.1 below). For the GS and GM models, this type of problem is obtained by taking the limit  $D \rightarrow \infty$  with  $\tau = 0$  in the GS model (1.5) and the GM model (1.7). A similar nonlocal model has been analyzed in detail in the context of hot-spot patterns arising in the microwave heating of ceramic materials (cf. [2], [3], [13]). The first observation and formal analysis of growing alternating-sign fluctuations for an activator-type variable in a reaction-diffusion system was given in [16] and [15] (see Sections 14.4.8, 15.3, Fig. 14.13, and Fig 14.16 of [15]). In [15] this phenomena was referred to as activator re-pumping. For the Brusselator model, and in a parameter regime similar to the intermediate range for the GS model, it was shown in [16] (see also Chapter 15 of [15]) that a periodic spike pattern can lose its stability to an alternating-sign fluctuation of the activator concentration if the period of the pattern is below some asymptotically small critical value. For the Brusselator, a scaling law for this minimum distance is given in equation (15.58) of [15], and has a similar form to the scaling law for a competition instability derived in §4 for the GS model in the intermediate regime.

In §5 we give a precise discussion of the relationship between our results and previous results on the GS model. The previous equilibrium and spectral results for the GS model in [6], [7], [8], [4], and [5], have been based on a different dimensionless form of the GS model. This alternative approach is presented and discussed in some detail in §5. In §4 and §3.4, and more briefly in §5, we also relate our results to those in [25]. The main conclusion is that our results have a clear overlap with these previous results only in the intermediate parameter regime for  $\mathcal{A}$  and for the infinite-line problem. Our analysis of synchronous spike oscillations and competition instabilities in the low feed-rate regime, which occur on a finite domain, is new. In §5 we also list a few open problems.

Since we only consider eigenvalues for which  $\lambda = O(1)$  as  $\varepsilon \rightarrow 0$ , we emphasize that our stability results are valid only for time intervals of  $O(1)$  as  $\varepsilon \rightarrow 0$ . To obtain stability results for unbounded time intervals, one must consider the stability of the symmetric  $k$ -spike solution with respect to the small translational eigenvalues of order  $\lambda = O(\varepsilon^2)$  in the spectrum of the linearization. Additional stability thresholds, with respect to the dimensionless parameters, occur for this class of eigenvalues. These eigenvalues are closely related to the existence of asymmetric  $k$ -spike solutions. This problem is studied in [18]. In Fig. 1 these additional thresholds correspond to the intersection points of the solid and heavy solid curves.

Finally, we make some remarks concerning the mathematical rigor of our approach. In §2 and §3 we only present a formal asymptotic derivation of the existence of equilibrium solutions in the low feed-rate regime in Principal Result 2.1 and a formal derivation of the nonlocal eigenvalue problem (NLEP) in Principal Result 3.2. However, starting with the NLEP of Principal Result 3.2, all of the spectral results of §3.2 for this eigenvalue problem have been rigorously established. Our stability conclusions of the formally constructed equilibrium solution are based on the spectral properties of this NLEP. However, since the

GM model and the GS model in the low feed-rate regime have a related asymptotic structure, a similar Lyapunov-Schmidt reduction analysis as was given for the GM model in [41] could be used to rigorously construct the equilibrium solution and to derive the nonlocal eigenvalue problem. An alternative method to construct periodic or homoclinic equilibrium solutions in the GS model is to use geometric singular perturbation theory both rigorously (cf. [8], [7]) or formally (cf. [6]).

## 2 Symmetric $k$ -Spike Equilibria: $\mathcal{A} = O(1)$

For  $\varepsilon \rightarrow 0$ , and with  $\mathcal{A} = O(1)$  and  $D = O(1)$ , we construct a symmetric  $k$ -spike equilibrium solution to (1.5) using matched asymptotic analysis. For this pattern the spike locations satisfy

$$x_j = -1 + \frac{(2j-1)}{k}, \quad j = 1, \dots, k. \quad (2.1)$$

For a symmetric spike pattern the spikes have equal height so that  $u(x_j) = U$  for  $j = 1, \dots, k$ .

Since the asymptotic construction of such a solution is similar to that done in [14] for the GM model, we will only sketch the formal derivation of the result. In §4, where we consider the intermediate regime  $O(1) \ll \mathcal{A} \ll O(\varepsilon^{-1/2})$ , we will give a detailed formal derivation of the equilibrium solutions for (1.2) and (1.5) and include formal error estimates associated with the inner and outer expansions.

In the inner region near the  $j^{\text{th}}$  spike, we let  $y = \varepsilon^{-1}(x - x_j)$ . In each inner region, we obtain that  $u \sim U + O(\varepsilon)$ . Therefore, from (1.5a), the leading-order inner solution for  $\nu$  is  $\nu \sim w/(\mathcal{A}U)$ , where  $w(y) = \frac{3}{2}\text{sech}^2(y/2)$  is the homoclinic solution to

$$w'' - w + w^2 = 0, \quad -\infty < y < \infty; \quad w \rightarrow 0 \quad \text{as} \quad |y| \rightarrow \infty, \quad w'(0) = 0, \quad w(0) > 0. \quad (2.2)$$

In the outer region, defined away from an  $O(\varepsilon)$  region near each spike,  $\nu$  is exponentially small and the term  $\varepsilon^{-1}u\nu^2$  in (1.5b) can be approximated by a Dirac mass. Thus, the outer solution for  $u$  satisfies

$$Du_{xx} + (1 - u) - \frac{6}{\mathcal{A}^2 U} \sum_{j=1}^k \delta(x - x_j) = 0, \quad -1 < x < 1; \quad u_x(\pm 1) = 0. \quad (2.3)$$

In obtaining (2.3), we used  $\int_{-\infty}^{\infty} w^2 dy = 6$ . The solution to (2.3) is

$$u(x) = 1 - \frac{6}{\mathcal{A}^2 U} \sum_{j=1}^k G(x; x_j), \quad (2.4)$$

where  $G(x; x_j)$  is the Green's function, satisfying

$$DG_{xx} - G = -\delta(x - x_j), \quad -1 < x < 1; \quad G_x(\pm 1; x_j) = 0. \quad (2.5)$$

A simple calculation gives,

$$G(x; x_j) = \begin{cases} g_j \cosh[\theta_0(1+x)] / \cosh[\theta_0(1+x_j)], & -1 < x < x_j, \\ g_j \cosh[\theta_0(1-x)] / \cosh[\theta_0(1-x_j)], & x_j < x < 1, \end{cases} \quad (2.6a)$$

where

$$g_j \equiv \frac{1}{\sqrt{D}} (\tanh [\theta_0(1 - x_j)] + \tanh [\theta_0(1 + x_j)])^{-1}, \quad \theta_0 \equiv D^{-1/2}. \quad (2.6b)$$

We define  $a_g \equiv \sum_{i=1}^k G(x_j; x_i)$ , where the spike locations satisfy (2.1). Using (2.6), we calculate

$$a_g \equiv \sum_{i=1}^k G(x_j; x_i) = \left[ 2\sqrt{D} \tanh (\theta_0/k) \right]^{-1}. \quad (2.7)$$

Therefore,  $a_g$  is independent of  $j$ . Setting  $u(x_j) = U$  in (2.4) we obtain a quadratic equation for  $U$

$$U(U - 1) = -\frac{6a_g}{\mathcal{A}^2}. \quad (2.8)$$

In this way, we obtain the following formal result for symmetric  $k$ -spike equilibrium solutions to (1.5):

**Principal Result 2.1:** *Let  $\varepsilon \rightarrow 0$ , with  $\mathcal{A} = O(1)$  and  $D = O(1)$  in (1.5). Then, when  $\mathcal{A} > \mathcal{A}_{ke}$ , there are two symmetric  $k$ -spike equilibrium solutions to (1.5) given asymptotically by*

$$\nu_{\pm}(x) \sim \frac{1}{\mathcal{A}U_{\pm}} \sum_{j=1}^k w[\varepsilon^{-1}(x - x_j)], \quad u_{\pm}(x) \sim 1 - \frac{(1 - U_{\pm})}{a_g} \sum_{j=1}^k G(x; x_j). \quad (2.9)$$

We label  $u_+$ ,  $\nu_+$  and  $u_-$ ,  $\nu_-$  as the small and large solution, respectively. In (2.9),  $w$  and  $G$  satisfy (2.2) and (2.5), respectively. In addition,  $U_{\pm}$  are the roots of (2.8) for  $\mathcal{A} > \mathcal{A}_{ke}$  given by

$$U_{\pm} = \frac{1}{2} \left[ 1 \pm \sqrt{1 - \frac{\mathcal{A}_{ke}^2}{\mathcal{A}^2}} \right], \quad \mathcal{A}_{ke} \equiv \sqrt{\frac{12\theta_0}{\tanh(\theta_0/k)}}, \quad \theta_0 \equiv D^{-1/2}. \quad (2.10)$$

The existence threshold  $\mathcal{A}_{ke}$ , representing a saddle-node bifurcation point for a  $k$ -spike solution on a finite domain, is a new result. These existence thresholds correspond to the fold points in Fig. 1 separating the upper and lower branches of symmetric  $k$ -spike equilibria. As a remark,  $\mathcal{A}_{ke}$  is an increasing function of  $k$ . For  $D \ll 1$  and with  $\sqrt{D}k \ll 1$ , we get  $\mathcal{A}_{ke} \sim \sqrt{12}D^{-1/4}$ . Thus, when  $D \ll 1$ , the existence threshold  $\mathcal{A}_{ke}$  is roughly independent of  $k$  provided that  $\sqrt{D}k \ll 1$ .

To display our results graphically, we introduce the  $L_2$  norm  $|\nu|_2$ . Using (2.9) and (2.10), we obtain

$$|\nu|_2 \equiv \left( \varepsilon^{-1} \int_{-1}^1 \nu^2 dx \right)^{1/2} \sim \frac{2\sqrt{6k}}{\mathcal{A}} \left[ 1 \pm \sqrt{1 - \frac{\mathcal{A}_{ke}^2}{\mathcal{A}^2}} \right]^{-1}. \quad (2.11)$$

For  $\mathcal{A} = 9.0$  and  $\varepsilon = 0.02$ , in Fig. 4(a) and Fig. 4(b) we plot the large solution when  $D = 0.75$  and  $D = 0.1$ , respectively. Notice that as  $D$  decreases, the Green's function in (2.9) decays more rapidly away from the spike locations. Hence, for  $D$  small,  $u$  should approach  $u \sim 1$  in the outer regions. This asymptotic value  $u \sim 1$  in the outer region is also relevant to the infinite-line problem, corresponding to a one-spike solution to (1.5) on  $-\infty < x < \infty$ . However, as seen from Fig. 4(b), even with  $D = 0.1$ ,  $u$  is not so close to its asymptotic value in the outer regions. Therefore, this suggests that there is range of values of  $D$  for which boundary effects due to the finite domain will be important in the analysis.



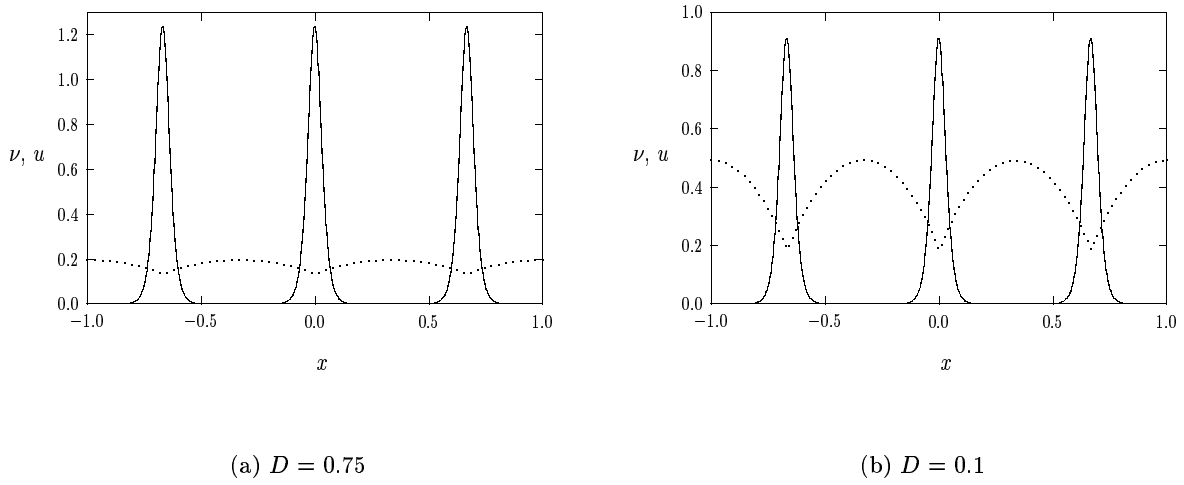


Figure 4: Large solution when  $k = 3$ ,  $\mathcal{A} = 9.0$ , and  $\varepsilon = 0.02$ . Left figure:  $D = 0.75$ . Right figure:  $D = 0.1$ .

The classification of small and large solution refers to low and high concentrations of  $\nu$  in the core of the spike. Smaller concentrations of  $u$  in the core of the spike generate larger amplitudes for  $\nu$ . Hence, each upper branch (upper solid curve) in Fig. 1 corresponds to the large solution, while each lower branch corresponds to the small solution. As shown in §3–§4, a convenient way to parameterize these solution branches is to introduce a parameter  $s$  defined by  $s \equiv (1 - U_{\pm})/U_{\pm}$ . Then, from (2.10), we get

$$\mathcal{A} = \mathcal{A}_{ke} \frac{(1+s)}{2\sqrt{s}}, \quad s = \frac{1 - U_{\pm}}{U_{\pm}}, \quad 0 < s < \infty. \quad (2.12)$$

Hence the large solution  $u_-$ ,  $\nu_-$  corresponds to the range  $1 < s < \infty$ , while the small solution  $u_+$ ,  $\nu_+$  corresponds to  $0 < s < 1$ . The existence threshold  $\mathcal{A}_{ke}$  corresponds to  $s = 1$ .

To analyze the stability of symmetric  $k$ -spike equilibrium solutions we let

$$u(x, t) = u_{\pm}(x) + e^{\lambda t} \eta(x), \quad \nu(x, t) = \nu_{\pm}(x) + e^{\lambda t} \phi(x), \quad (2.13)$$

where  $\eta \ll 1$  and  $\phi \ll 1$ . Substituting (2.13) into (1.5) and linearizing, we obtain the eigenvalue problem

$$\varepsilon^2 \phi_{xx} - \phi + 2\mathcal{A}u_{\pm}\nu_{\pm}\phi + \mathcal{A}\eta\nu_{\pm}^2 = \lambda\phi, \quad -1 < x < 1; \quad \phi_x(\pm 1) = 0, \quad (2.14a)$$

$$D\eta_{xx} - \eta - \varepsilon^{-1}\nu_{\pm}^2\eta - 2\varepsilon^{-1}u_{\pm}\nu_{\pm}\phi = \tau\lambda\eta, \quad -1 < x < 1; \quad \eta_x(\pm 1) = 0. \quad (2.14b)$$

In §3 we analyze the spectrum of (2.14) corresponding to those eigenfunctions that are not locally odd functions near each spike. The corresponding eigenvalues, which determine the stability of the symmetric  $k$ -spike solution with respect to instabilities occurring on a fast  $O(1)$  time-scale, are referred to as the large eigenvalues. We will show that the small solution  $u_+$  and  $\nu_+$  is always unstable. For the large solution, we show that there are two different types of instabilities that can occur depending on the parameter ranges of  $D$ ,  $\mathcal{A}$ ,  $\tau$ , and  $k$ . A competition instability, whereby spikes in a spike sequence are destroyed, can occur

only for  $k > 1$  when  $\mathcal{A}$  is close to  $\mathcal{A}_{ke}$ . This instability results from a certain eigenvalue on the positive real axis  $\text{Re}(\lambda) > 0$ . On the other hand, oscillatory instabilities in the amplitudes of the spikes as a result of a Hopf bifurcation can occur for any  $\mathcal{A} > \mathcal{A}_{ke}$  when  $\tau$  is sufficiently large.

### 3 Large Eigenvalues: Fast Profile Instabilities for $\mathcal{A} = O(1)$

We now study the stability of the equilibrium solutions of Principal Result 2.1 on an  $O(1)$  time-scale.

#### 3.1 The Nonlocal Eigenvalue Problem

We begin by deriving a nonlocal eigenvalue problem that is central to the analysis. This derivation is similar to that of [39] for the GM model (1.7), and is related to the approach used in [29] to analyze pulse stability in the Fitzhugh-Nagumo system. We look for a localized eigenfunction for  $\phi$  in (2.14) in the form

$$\phi(x) \sim \sum_{j=1}^k c_j \Phi[\varepsilon^{-1}(x - x_j)] , \quad (3.1)$$

for some coefficients  $c_j$ . As shown below, these coefficients are related to the eigenvectors of a certain matrix eigenvalue problem. The large eigenvalues are characterized by the condition that  $\int_{-\infty}^{\infty} w(y)\Phi(y) dy \neq 0$ .

Since  $\phi$  is localized near each  $x_j$ , the spatially inhomogeneous coefficients in (2.14b) can be approximated by Dirac masses. In this way, we use (3.1), (2.9), and  $\int_{-\infty}^{\infty} w^2 dy = 6$ , to obtain for  $x \sim x_j$  that

$$\varepsilon^{-1}\nu_{\pm}^2 \sim \frac{6}{\mathcal{A}^2 U_{\pm}^2} \delta(x - x_j) , \quad 2\varepsilon^{-1}u_{\pm}\nu_{\pm}\phi \sim \frac{2c_j}{\mathcal{A}} \left( \int_{-\infty}^{\infty} w(y)\Phi(y) dy \right) \delta(x - x_j) . \quad (3.2)$$

Here  $\delta(x)$  is the delta function. Substituting (3.2) into (2.14b), we get that  $\eta$  satisfies

$$D\eta_{xx} - \left( 1 + \tau\lambda + \frac{6}{\mathcal{A}^2 U_{\pm}^2} \sum_{i=1}^k \delta(x - x_i) \right) \eta = \frac{2}{\mathcal{A}} \left( \int_{-\infty}^{\infty} w\Phi dy \right) \sum_{i=1}^k c_i \delta(x - x_i) , \quad |x| < 1 , \quad (3.3)$$

with  $\eta_x(\pm 1) = 0$ . Defining  $[\xi]_i$  by  $[\xi]_i \equiv \xi(x_{i+}) - \xi(x_{i-})$ , we obtain that this problem is equivalent to

$$D\eta_{xx} - (1 + \tau\lambda)\eta = 0 , \quad |x| \leq 1 ; \quad \eta_x(\pm 1) = 0 , \quad (3.4a)$$

$$[\eta]_i = 0 , \quad [D\eta_x]_i = -\omega_i + \frac{6}{\mathcal{A}^2 U_{\pm}^2} \eta(x_i) , \quad i = 1, \dots, k ; \quad \omega_i \equiv -\frac{2c_i}{\mathcal{A}} \int_{-\infty}^{\infty} w(y)\Phi(y) dy . \quad (3.4b)$$

To determine the eigenvalue problem for  $\lambda$ , we first need to compute  $\eta(x_i)$  from (3.4). To do so, we solve (3.4a) on each subinterval and use the jump conditions (3.4b) to patch the solution together across each subinterval. This calculation results in the matrix problem

$$\mathcal{B}\eta = [(1 + \tau\lambda)D]^{-1/2} \omega , \quad \omega = -\frac{2c}{\mathcal{A}} \int_{-\infty}^{\infty} w(y)\Phi(y) dy . \quad (3.5)$$

Here we have defined the vectors  $\boldsymbol{\omega}$ ,  $\mathbf{c}$ , and  $\boldsymbol{\eta}$ , by  $\boldsymbol{\omega}^t = (\omega_1, \dots, \omega_k)$ ,  $\mathbf{c}^t = (c_1, \dots, c_k)$ , and  $\boldsymbol{\eta}^t = (\eta_1, \dots, \eta_k)$ , where  $t$  denotes transpose. The matrix  $\mathcal{B}$  in (3.5) is given in terms of a tridiagonal matrix  $\mathcal{B}_0$  by

$$\mathcal{B} = \mathcal{B}_0 + \frac{6}{\mathcal{A}^2 U_{\pm}^2 \sqrt{(1 + \tau\lambda)D}} I, \quad \mathcal{B}_0 \equiv \begin{pmatrix} d_{\lambda} & f_{\lambda} & 0 & \cdots & 0 & 0 & 0 \\ f_{\lambda} & e_{\lambda} & f_{\lambda} & \cdots & 0 & 0 & 0 \\ 0 & f_{\lambda} & e_{\lambda} & \ddots & 0 & 0 & 0 \\ \vdots & \vdots & \ddots & \ddots & \ddots & \vdots & \vdots \\ 0 & 0 & 0 & \ddots & e_{\lambda} & f_{\lambda} & 0 \\ 0 & 0 & 0 & \cdots & f_{\lambda} & e_{\lambda} & f_{\lambda} \\ 0 & 0 & 0 & \cdots & 0 & f_{\lambda} & d_{\lambda} \end{pmatrix}. \quad (3.6)$$

Here  $I$  is the  $k \times k$  identity matrix, and the matrix entries of  $\mathcal{B}_0$  are

$$d_{\lambda} \equiv \coth\left(\frac{2\theta_{\lambda}}{k}\right) + \tanh\left(\frac{\theta_{\lambda}}{k}\right); \quad e_{\lambda} \equiv 2 \coth\left(\frac{2\theta_{\lambda}}{k}\right); \quad f_{\lambda} \equiv -\operatorname{csch}\left(\frac{2\theta_{\lambda}}{k}\right). \quad (3.7)$$

In (3.7),  $\theta_{\lambda}$  is the principal branch of the square root defined by  $\theta_{\lambda} \equiv \theta_0 \sqrt{1 + \tau\lambda}$ , with  $\theta_0 \equiv D^{-1/2}$ .

Next, we substitute (3.1) and (3.6) into (2.14a). This yields the nonlocal eigenvalue problem

$$c_i \left( \Phi'' - \Phi + 2w\Phi \right) - \frac{12w^2}{\mathcal{A}^2 U_{\pm}^2} [(1 + \tau\lambda) D]^{-1/2} (\mathcal{B}^{-1} \mathbf{c})_i \left( \frac{\int_{-\infty}^{\infty} w \Phi dy}{\int_{-\infty}^{\infty} w^2 dy} \right) = \lambda c_i \Phi, \quad (3.8)$$

with  $\Phi(y) \rightarrow 0$  as  $|y| \rightarrow \infty$ . Therefore, we must calculate the spectrum of the matrix eigenvalue problem

$$\mathcal{B} \mathbf{c} = \kappa \mathbf{c}, \quad \kappa = \kappa_0 + \frac{6}{\mathcal{A}^2 U_{\pm}^2} [(1 + \tau\lambda) D]^{-1/2}, \quad (3.9)$$

where  $\kappa_0$  and  $\mathbf{c}$  is an eigenpair of  $\mathcal{B}_0$ . These eigenpairs were calculated explicitly in Proposition 2 of [14].

**Lemma 3.1:** *The eigenvalues  $\kappa_{0j}$ , with  $0 < \kappa_{01} < \dots < \kappa_{0k}$ , and the normalized eigenvectors  $\mathbf{c}_j$  of  $\mathcal{B}_0$  are*

$$\kappa_{0j} = 2 \tanh(\theta_{\lambda}/k) + 2 \left[ 1 - \cos\left(\frac{\pi(j-1)}{k}\right) \right] \operatorname{csch}(2\theta_{\lambda}/k), \quad j = 1, \dots, k, \quad (3.10a)$$

$$\mathbf{c}_1^t = \frac{1}{\sqrt{k}} (1, \dots, 1); \quad c_{l,j} = \sqrt{\frac{2}{k}} \cos\left(\frac{\pi(j-1)}{k} (l-1/2)\right), \quad j = 2, \dots, k. \quad (3.10b)$$

Here  $\mathbf{c}^t$  denotes transpose and  $\mathbf{c}_j^t = (c_{1,j}, \dots, c_{k,j})$ .

Substituting (3.9) and (3.10) into (3.8), we formally obtain the following spectral problem for the large  $O(1)$  eigenvalues of (2.14):

**Principal Result 3.2:** *For  $0 < \varepsilon \ll 1$ , the  $O(1)$  eigenvalues of (2.14) satisfy the NLEP*

$$L_0 \Phi - \chi w^2 \left( \frac{\int_{-\infty}^{\infty} w \Phi dy}{\int_{-\infty}^{\infty} w dy} \right) = \lambda \Phi, \quad -\infty < y < \infty; \quad \Phi \rightarrow 0, \quad \text{as } |y| \rightarrow \infty. \quad (3.11a)$$

Here the operator  $L_0$ , referred to as the local operator, is defined by

$$L_0 \Phi \equiv \Phi'' - \Phi + 2w\Phi. \quad (3.11b)$$

In (3.11a) there are  $k$  choices for the multiplier  $\chi = \chi(z; j)$ , for  $j = 1, \dots, k$ , given explicitly by

$$\chi = \chi(z; j) \equiv 2s \left( s + \frac{\sqrt{1+z}}{\tanh(\theta_0/k)} \left[ \tanh(\theta_\lambda/k) + \frac{(1 - \cos[\pi(j-1)/k])}{\sinh(2\theta_\lambda/k)} \right] \right)^{-1}, \quad (3.12a)$$

where

$$z \equiv \tau\lambda, \quad \theta_\lambda \equiv \theta_0\sqrt{1+z}, \quad \theta_0 \equiv D^{-1/2}, \quad s \equiv \frac{1 - U_\pm}{U_\pm}. \quad (3.12b)$$

Here  $U_\pm$  is determined in terms of  $\mathcal{A}/\mathcal{A}_{ke}$  by (2.10). The global eigenfunction  $\phi(x)$  is given by (3.1), where the coefficients  $\mathbf{c}^t = (c_1, \dots, c_k)$  are the eigenvectors of  $\mathcal{B}_0$  given in (3.10b).

We now establish a spectral equivalence principle between the NLEP (3.11) and a corresponding NLEP derived in the formal Proposition 2.3 of [39] for the GM model (1.7) with exponent set  $(p, q, m, s)$ . Proposition 2.3 of [39] shows that the nonlocal eigenvalue problem for the GM model with exponent set  $(2, q, 2, s)$  has exactly the same form as in (3.11), except that  $\chi$  in (3.12) is to be replaced with

$$\chi = \chi(z; j) \equiv 2q \left( s + \frac{\sqrt{1+z}}{\tanh(\theta_0/k)} \left[ \tanh(\theta_\lambda/k) + \frac{(1 - \cos[\pi(j-1)/k])}{\sinh(2\theta_\lambda/k)} \right] \right)^{-1}. \quad (3.13)$$

Therefore, the nonlocal eigenvalue problems for the GM model and the GS model are identical if we take  $q = s$ , to get the GM exponent set  $(p, q, m, s) = (2, s, 2, s)$ , where  $s$  is given in (3.12b). However, in the GM model, the exponents  $(p, q, m, s)$  generally satisfy  $\zeta \equiv qm/(p-1) - (1+s) > 0$  (see (1.8)). The spectral results in [39] for the GM model were obtained under this condition. With the exponent set  $(2, s, 2, s)$ , we calculate  $\zeta = s - 1$ . Since  $0 < s < 1$  corresponds to the small solution, while  $s > 1$  corresponds to the large solution, we obtain the following spectral equivalence principle:

**Proposition 3.3:** *In the limit  $\varepsilon \ll 1$ , consider the large eigenvalues of (2.14). The nonlocal eigenvalue problem for the stability of the large  $k$ -spike symmetric equilibrium solution  $u_-$ ,  $\nu_-$  of the GS model (1.5) is identical to the related nonlocal eigenvalue problem for the GM model (1.7) with exponent set  $(p, q, m, s) = (2, s, 2, s)$ , where  $s > 1$  is given in (3.12b). The spectral problem for the small solution of the GS model is also equivalent to that for a GM model with exponents  $(2, s, 2, s)$ , except that  $\zeta < 0$  in (1.8).*

For the GS model (1.5), the NLEP (3.11) is a new result. Proposition 3.3 allows us to analyze the stability of the large solution of the GS model by directly appealing to some results of [39] obtained for the GM model with arbitrary exponent set  $(p, q, m, s)$  satisfying (1.8). For the small solution  $u_+$ ,  $\nu_+$ , we must extend the analysis in [39] to allow for a GM model with exponent set  $(2, s, 2, s)$ , where  $\zeta = s - 1 < 0$ .

Next, we reformulate (3.11) into a form more amenable to analysis. Let  $\psi(y)$  be the solution to

$$L_0\psi \equiv \psi'' - \psi + 2w\psi = \lambda\psi + w^2; \quad \psi \rightarrow 0 \quad \text{as} \quad |y| \rightarrow \infty. \quad (3.14)$$

Then, the eigenfunctions of (3.11) can be written as

$$\Phi = \chi(\tau\lambda; j)\psi J, \quad J \equiv \frac{\int_{-\infty}^{\infty} w\Phi dy}{\int_{-\infty}^{\infty} w^2 dy}. \quad (3.15)$$

Using (3.15), and assuming that  $\int_{-\infty}^{\infty} w\Phi dy \neq 0$ , we then obtain that the eigenvalues of (3.11) are the union of the zeros of the functions  $g_j(\lambda) = 0$  for  $j = 1, \dots, k$ , where

$$g_j(\lambda) \equiv C_j(\lambda) - f(\lambda), \quad f(\lambda) \equiv \frac{\int_{-\infty}^{\infty} w(L_0 - \lambda)^{-1} w^2 dy}{\int_{-\infty}^{\infty} w^2 dy}. \quad (3.16)$$

Here we have defined  $C_j(\lambda) \equiv [\chi(\tau\lambda; j)]^{-1}$ , for  $j = 1, \dots, k$ , so that from (3.12a) we obtain

$$C_j(\lambda) = \frac{1}{2} + \frac{\sqrt{1 + \tau\lambda}}{2s \tanh(\theta_0/k)} \left[ \tanh(\theta_\lambda/k) + \frac{(1 - \cos[\pi(j-1)/k])}{\sinh(2\theta_\lambda/k)} \right]. \quad (3.17)$$

After establishing the theoretical results in §3.2, in §3.3 we numerically determine the roots of (3.16) by following a similar approach as in [39]. We use a combination of Newton's method coupled to the numerical solution to the boundary value problem (3.14) obtained by COLSYS [1]. Although (3.14) can be solved explicitly in terms of hypergeometric functions (cf. [6]), we do not follow this approach since with these special functions it is then difficult to prove rigorous results for the spectrum of (3.11).

### 3.2 Theoretical Results on the Spectrum: Large Eigenvalues

We now give rigorous results for the spectrum of the NLEP (3.11). We begin by looking for roots of (3.16) on the non-negative real axis  $\lambda = \lambda_R \geq 0$ . The first observation is that  $f(\lambda_R)$  has a singularity on the positive real axis as a consequence of Theorem 2.12 of [21].

**Lemma 3.4:** (From [21]): *Consider the local eigenvalue problem  $L_0\phi_l = \sigma\phi_l$  for  $\phi_l \in \mathcal{H}^1(R)$ . This problem admits the eigenvalues  $\sigma_0 > 0$ ,  $\sigma_1 = 0$ , and  $\sigma_j < 0$  for  $j > 1$ . The eigenvalue  $\sigma_0$  is simple, and the corresponding eigenfunction  $\phi_{l0}$  has one sign. The unstable eigenvalue is  $\sigma_0 = 5/4$ .*

Since  $\sigma_0 > 0$ , then  $f(\lambda_R) \rightarrow +\infty$  as  $\lambda_R \rightarrow \sigma_0^-$ . In [39] the behavior of  $f(\lambda_R)$  on the positive real axis was studied. The following rigorous result is a consequence of Proposition 3.5 of [39]:

**Proposition 3.5:** (From [39]): *For  $\lambda_R \geq 0$ , the function  $f(\lambda_R)$  in (3.16) has the local behavior,*

$$f(\lambda_R) \sim 1 + \frac{3\lambda_R}{4} + \kappa_c \lambda_R^2 + O(\lambda_R^3), \quad \text{as } \lambda_R \rightarrow 0; \quad \kappa_c \equiv \frac{\int_{-\infty}^{\infty} (L_0^{-1}w)^2 dy}{\int_{-\infty}^{\infty} w^2 dy} > 0. \quad (3.18a)$$

In addition, we have the global behavior  $f(\lambda_R) \rightarrow +\infty$  as  $\lambda_R \rightarrow \sigma_0^-$ , and

$$f'(\lambda_R) > 0, \quad f''(\lambda_R) > 0, \quad \text{for } 0 < \lambda_R < \sigma_0; \quad f(\lambda_R) < 0, \quad \text{for } \lambda_R > \sigma_0. \quad (3.18b)$$

**Proof:** This result is simply Proposition 3.5 of [39] for a GM model with exponents  $p = m = 2$ . ■

Next, we summarize the key properties of  $C_j(\lambda)$  when  $\lambda = \lambda_R \geq 0$  is real.

**Proposition 3.6:** *For any fixed  $\tau > 0$ , we have a monotonicity result for  $\lambda_R \geq 0$  that*

$$C_k(\lambda_R) > C_{k-1}(\lambda_R) > \dots > C_1(\lambda_R) > 0, \quad C'_k(\lambda_R) < C'_{k-1}(\lambda_R) < \dots < C'_1(\lambda_R). \quad (3.19a)$$

In addition, for  $\tau > 0$ , and for each  $j = 1, \dots, k$ , we have for  $\lambda_R > 0$  that

$$C'_j(\lambda_R) > 0, \quad C''_j(\lambda_R) < 0, \quad C'_j(\lambda_R) = O(\tau^{1/2}), \quad \text{as } \tau \rightarrow +\infty. \quad (3.19b)$$

Define  $B_j$  by  $B_j = C_j(0)$  for  $j = 1, \dots, k$ . These coefficients are independent of  $\tau$  and satisfy

$$\frac{(s+1)}{2s} = B_1 < B_2 < \dots < B_k; \quad \frac{dB_j}{dD} > 0, \quad j = 2, \dots, k; \quad \frac{dB_j}{ds} < 0, \quad j = 1, \dots, k. \quad (3.19c)$$

**Proof:** This is Proposition 5.1 of [39] for a GM model with exponents  $(p, q, m, s) = (2, s, 2, s)$ . The monotonicity result for  $B_j$  with respect to  $s$  is immediate from (3.17). ■

As shown below, the critical values of  $D$  and  $\mathcal{A}$  where  $B_j = 1$  for  $j = 2, \dots, k$  play a central role in the analysis. We now calculate these values. The first observation is that for the small solution branch where  $0 < s < 1$ , we have from (3.19c) that  $B_j > 1$  for  $j = 1, \dots, k$ . Therefore,

$$1 < C_1(0) < C_2(0) < \dots < C_k(0), \quad \text{for } 0 < s < 1. \quad (3.20)$$

For the large solution branch where  $s > 1$  we calculate the values  $D = D_j$  for which  $B_j = C_j(0) = 1$  for  $j = 2, \dots, k$ . Since  $B_1 < 1$  for any  $D$ , there is no threshold value  $D_1$ . Using (3.17) we calculate

$$B_j = \frac{1}{2} \left( 1 + \frac{1}{s} \right) + \frac{\gamma_j}{4s \sinh^2(\theta_0/k)}, \quad \gamma_j \equiv 1 - \cos \left( \frac{\pi(j-1)}{k} \right). \quad (3.21)$$

Setting  $B_j = 1$ , for  $j = 2, \dots, k$ , and solving for the thresholds  $D_j$ , we get

$$D_j \equiv \frac{4}{k^2 \left[ \ln \left( r_j + \sqrt{r_j^2 - 1} \right) \right]^2}, \quad j = 2, \dots, k; \quad r_j \equiv \frac{\gamma_j}{s-1} + 1, \quad j = 2, \dots, k. \quad (3.22)$$

Alternatively, for a fixed  $D$ , we can calculate thresholds  $\mathcal{A} = \mathcal{A}_j$  for which  $B_j = 1$ . Using (2.12), which relates  $s$  in terms of  $\mathcal{A}$ , we then set  $B_j = 1$  in (3.21) to obtain

$$\mathcal{A}_j = \mathcal{A}_{ke} \frac{[(\gamma_j/2) + 2 \sinh^2(\theta_0/k)]}{\left( [(\gamma_j/2) + 2 \sinh^2(\theta_0/k)]^2 - (\gamma_j/2)^2 \right)^{1/2}}, \quad j = 2, \dots, k. \quad (3.23)$$

Here  $\mathcal{A}_{ke}$  are the existence thresholds of (2.10). Using (3.19c), (3.22), and (3.23), we then show that

$$\mathcal{A}_2 < \mathcal{A}_3 < \dots < \mathcal{A}_k, \quad D_k < D_{k-1} < \dots < D_2. \quad (3.24)$$

Therefore,  $B_j < 1$  for  $j = 2, \dots, k$  whenever  $D < D_k$  or when  $\mathcal{A} > \mathcal{A}_k$ . We label these critical values by

$$D_k \equiv D_{kL} \equiv \frac{4}{k^2 \left[ \ln \left( r_k + \sqrt{r_k^2 - 1} \right) \right]^2}, \quad r_k \equiv \frac{\gamma_k}{s-1} + 1, \quad (3.25a)$$

$$\mathcal{A}_k \equiv \mathcal{A}_{kL} \equiv \mathcal{A}_{ke} \frac{((\gamma_k/2) + 2 \sinh^2(\theta_0/k))}{\left( [(\gamma_k/2) + 2 \sinh^2(\theta_0/k)]^2 - (\gamma_k/2)^2 \right)^{1/2}}, \quad \gamma_k \equiv 1 + \cos \left( \frac{\pi}{k} \right). \quad (3.25b)$$

Next, we look for roots of (3.16) on the non-negative imaginary axis  $\lambda = i\lambda_I$ , with  $\lambda_I \geq 0$ . Substituting  $\lambda = i\lambda_I$  into (3.14) and (3.16), and extracting real and imaginary parts, we obtain that the eigenvalues of (3.11) with  $\lambda = i\lambda_I$  and  $\lambda_I \geq 0$  are the roots of the coupled system  $g_{Rj} = g_{Ij} = 0$ , where

$$g_{Rj}(\lambda_I) \equiv C_{Rj}(\lambda_I) - f_R(\lambda_I), \quad g_{Ij}(\lambda_I) \equiv C_{Ij}(\lambda_I) - f_I(\lambda_I), \quad j = 1, \dots, k. \quad (3.26a)$$

Here we have defined  $g_{Rj}(\lambda_I) \equiv \text{Re}[g_j(i\lambda_I)]$ ,  $g_{Ij}(\lambda_I) \equiv \text{Im}[g_j(i\lambda_I)]$ . In (3.26a), we have

$$f_R(\lambda_I) \equiv \frac{\int_{-\infty}^{\infty} w L_0 [L_0^2 + \lambda_I^2]^{-1} w^2 dy}{\int_{-\infty}^{\infty} w^2 dy}, \quad f_I(\lambda_I) \equiv \frac{\lambda_I \int_{-\infty}^{\infty} w [L_0^2 + \lambda_I^2]^{-1} w^2 dy}{\int_{-\infty}^{\infty} w^2 dy}, \quad (3.26b)$$

$$C_{Rj}(\lambda_I) \equiv \text{Re}[C_j(i\lambda_I)], \quad C_{Ij}(\lambda_I) \equiv \text{Im}[C_j(i\lambda_I)]. \quad (3.26c)$$

Some qualitative properties of the functions  $f_R$ ,  $f_I$ ,  $C_{Rj}$ , and  $C_{Ij}$  are summarized as follows:

**Proposition 3.7:** *The functions  $f_R$  and  $f_I$  in (3.26b) have the asymptotic behavior*

$$f_R(\lambda_I) \sim 1 - \kappa_c \lambda_I^2 + O(\lambda_I^4), \quad \text{as } \lambda_I \rightarrow 0; \quad f_R(\lambda_I) = O(\lambda_I^{-2}), \quad \text{as } \lambda_I \rightarrow \infty, \quad (3.27a)$$

$$f_I(\lambda_I) \sim \frac{3\lambda_I}{4} + O(\lambda_I^3), \quad \text{as } \lambda_I \rightarrow 0; \quad f_I(\lambda_I) = O(\lambda_I^{-1}), \quad \text{as } \lambda_I \rightarrow \infty. \quad (3.27b)$$

Here  $\kappa_c$  is given in (3.18a). Moreover, the functions  $f_R(\lambda_I)$  and  $f_I(\lambda_I)$  have the global behavior

$$f'_R(\lambda_I) < 0, \quad f_I(\lambda_I) > 0, \quad \text{for } \lambda_I > 0. \quad (3.27c)$$

For  $\lambda_I > 0$  and  $\tau > 0$ , the functions  $C_{Rj}$  and  $C_{Ij}$  satisfy

$$C_{Rj}(0) = B_j, \quad C'_{Rj}(\lambda_I) > 0; \quad C_{Ij}(0) = 0, \quad C'_{Ij}(\lambda_I) > 0, \quad (3.28a)$$

$$C'_{Rj}(\lambda_I) = O(\tau^{1/2}), \quad C'_{Ij}(\lambda_I) = O(\tau^{1/2}), \quad \text{as } \tau \rightarrow \infty, \quad (3.28b)$$

$$C_{Rj}(\lambda_I) = C_{Rj}(0) + O(\tau\lambda_I), \quad C_{Ij}(\lambda_I) = O(\tau\lambda_I), \quad \text{as } \tau \rightarrow 0. \quad (3.28c)$$

Here  $B_j$  are the values  $C_j(0) = B_j$ , whose properties were given in (3.19c).

**Proof:** The proof of (3.27) is a special case of Propositions 3.1 and 3.2 of [39] for the GM model (1.7) with  $p = m = 2$ . The proof of (3.28) follows from setting  $\lambda = i\lambda_I$  in the definition of  $C_j(\lambda)$  in (3.17). ■

To determine the number of eigenvalues in the unstable right half-plane  $\text{Re}(\lambda) > 0$  we calculate the winding number of  $g_j(\lambda)$  in (3.16), with  $\lambda = \lambda_R + i\lambda_I$ , over the counterclockwise contour composed of the imaginary axis  $-iR \leq \text{Im}\lambda \leq iR$  and the semi-circle  $\Gamma_R$ , given by  $|\lambda| = R > 0$ , for  $-\pi/2 \leq \arg\lambda \leq \pi/2$ . The function  $g_j(\lambda)$  in (3.16) is analytic in the right half-plane, except at the simple pole  $\lambda = \sigma_0 = 5/4 > 0$ , which is the unique positive eigenvalue of the operator  $L_0$  (see Lemma 3.4 above). For any  $\tau > 0$ , we have from (3.17) that  $C_j(\lambda) \sim O(\sqrt{\lambda})$  as  $|\lambda| \rightarrow \infty$  in the right half-plane. Moreover,  $f(\lambda) \rightarrow 0$  as  $|\lambda| \rightarrow \infty$ . Hence, for any  $\tau > 0$ , the change in the argument of  $g_j(\lambda)$  over  $\Gamma_R$  as  $R \rightarrow \infty$  is  $\pi/2$ . Therefore, assuming that there are no zeros of  $g_j(\lambda)$  on the imaginary axis, we let  $R \rightarrow \infty$  and use the argument principle together with  $g_j(\bar{\lambda}) = \overline{g_j(\lambda)}$  to obtain the following winding number criterion:

**Proposition 3.8:** *Let  $\tau > 0$  and assume that there are no zeros of  $g_j(\lambda)$  on the imaginary axis for  $j = 1, \dots, k$ . Then, the number of eigenvalues  $M$  of (3.11) in  $\text{Re}(\lambda) > 0$  satisfies*

$$M = \frac{5k}{4} + \frac{1}{\pi} \sum_{j=1}^k [\arg g_j]_{\Gamma_I}. \quad (3.29)$$

Here  $[\arg g_j]_{\Gamma_I}$  denotes the change in the argument of  $g_j(\lambda)$  along the semi-infinite imaginary axis  $\Gamma_I = i\lambda_I$ ,  $0 \leq \lambda_I < \infty$ , traversed in the downwards direction.

Using the properties given in Propositions 3.6 and 3.7, there are only a few possible values for  $[\arg g_j]_{\Gamma_I}$ . This leads to a more specific winding number criterion.

**Proposition 3.9:** *Let  $\tau > 0$ . Then, there are three distinct possibilities:*

$$(1): \text{ if } g_{Ij} < 0 \text{ when } g_{Rj} = 0, \quad \text{then } [\arg g_j]_{\Gamma_I} = -5\pi/4, \quad (3.30a)$$

$$(2): \text{ if } g_{Ij} > 0 \text{ when } g_{Rj} = 0, \quad \text{then } [\arg g_j]_{\Gamma_I} = 3\pi/4, \quad (3.30b)$$

$$(3): \text{ if } g_{Rj} > 0 \text{ for all } \lambda_I \geq 0, \quad \text{then } [\arg g_j]_{\Gamma_I} = -\pi/4. \quad (3.30c)$$

**Proof:** Let  $\tau > 0$ . From (3.28) and (3.27),  $C_{Rj}(\lambda_I)$  is a positive monotone increasing function and  $f_R(\lambda_I)$  is a positive monotone decreasing function. Therefore,  $g_{Rj} = 0$  has at most one root. First suppose that  $C_{Rj}(0) < f_R(0) = 1$  so that  $g_{Rj} = 0$  has a root. Then, using (3.28) and (3.27) we get  $g_{Rj} \sim b\sqrt{\lambda_I}$  and  $g_{Ij} \sim b\sqrt{\lambda_I}$  as  $\lambda_I \rightarrow +\infty$  for some  $b > 0$ . In addition, from (3.27b) and  $C_{Ij}(0) = 0$  it follows that  $g_{Rj} < 0$  and  $g_{Ij} = 0$  at  $\lambda_I = 0$ . Therefore,  $\arg g_j = \pi/4$  as  $\lambda_I \rightarrow +\infty$ , and  $\arg g_j = -\pi$  at  $\lambda_I = 0$ . Since the root to  $g_{Rj} = 0$  is unique, this shows that  $[\arg g_j]_{\Gamma_I}$  is either  $5\pi/4$  or  $-3\pi/4$  depending on the sign of  $g_{Ij}$  at the unique root of  $g_{Rj} = 0$ . This proves (3.30a) and (3.30b). Next, suppose that  $C_{Rj}(0) > f_R(0) = 1$ . Then, since  $g_{Rj}(0) > 0$  and  $g'_{Rj}(\lambda_I) > 0$  from (3.27c) and (3.28a), we conclude that  $g_{Rj} > 0$  for  $\lambda_I \geq 0$ . In this case,  $\arg g_j = 0$  at  $\lambda_I = 0$ . Since  $g_{Rj} > 0$  for all  $\lambda_I > 0$ , the result (3.30c) follows. ■

The first consequence of Propositions 3.5–3.9 concerns the stability of the small solution  $u_+$ ,  $\nu_+$ .

**Proposition 3.10:** *For any  $\tau > 0$ ,  $D > 0$ , and  $0 < s < 1$ , the small solution  $u_+$ ,  $\nu_+$  is unstable due to exactly  $k$  positive real eigenvalues of (3.11) located in the interval  $0 < \lambda_R < \sigma_0 = 5/4$ . These  $k$  unstable eigenvalues have a common leading-order asymptotic behavior as  $\tau \rightarrow \infty$*

$$\lambda_R \sim \frac{5}{4} + \frac{\delta_1}{\sqrt{\tau}} + \dots; \quad \delta_1 \equiv -\frac{4s \tanh(\theta_0/k)}{\sqrt{5}} \frac{\left( \int_{-\infty}^{\infty} w \phi_{l0} dy \right) \left( \int_{-\infty}^{\infty} w^2 \phi_{l0} dy \right)}{\int_{-\infty}^{\infty} w^2 dy}. \quad (3.31)$$

Here  $\phi_{l0}$  is the principal eigenfunction of  $L_0$  (see Lemma 3.4), normalized by  $\int_{-\infty}^{\infty} \phi_{l0}^2 dy = 1$ .

**Proof:** Let  $\tau > 0$  and  $0 < s < 1$ . Since  $C_{Rj}(0) = B_j > 1$  for  $j = 1, \dots, k$  from (3.20), we have  $g_{Rj}(0) > 0$ , and consequently  $g_{Rj}(\lambda_I) > 0$  for  $\lambda_I \geq 0$ . Therefore, for  $j = 1, \dots, k$ , condition (3) of Proposition 3.9 applies. From (3.29) this yields that there are  $M = k$  eigenvalues in the right half-plane for any  $\tau > 0$  and  $0 < s < 1$ . Next, we show that these eigenvalues are real and positive. For any  $0 < s < 1$ , (3.19c) yields that  $1 < B_1 < B_2 < \dots < B_k$ , and consequently  $1 = f(0) < C_1(0) < \dots < C_k(0)$ . Proposition 3.6 proves that  $C_j(\lambda_R)$  is a positive increasing and concave function, while  $f(\lambda_R)$  is a positive increasing convex function on  $0 \leq \lambda_R < \sigma_0$ . Hence, it follows that  $g_j(\lambda_R) = 0$  has exactly one root for each  $j = 1, \dots, k$  on the interval  $0 \leq \lambda_R < \sigma_0$ . Since  $f(\lambda_R) < 0$  for  $\lambda_R > \sigma_0$  from (3.18b), there can be no roots on  $\lambda_R > \sigma_0$ . Hence, we have  $k$  real positive eigenvalues for (3.11) on the interval  $0 < \lambda_R < \sigma_0 = 5/4$ . The asymptotic behavior (3.31) is obtained by expanding  $\lambda_R$  and  $\psi$  in fractional powers of  $\tau$  similar to that done in Proposition 3.8 of [39] for the GM model, and using  $C_j(\lambda_R) \sim c_\infty \tau^{1/2}$  for  $\tau \gg 1$  from (3.17). ■

The next result gives a criterion for the stability of a one-spike large solution  $u_-$ ,  $\nu_-$ , and for a  $k$ -spike large solution when  $D < D_{kL}$ , or  $\mathcal{A} > \mathcal{A}_{kL}$ . Here  $D_{kL}$  and  $\mathcal{A}_{kL}$  are the thresholds given in (3.25).

**Proposition 3.11** *Let  $\tau > 0$ ,  $k = 1$ , and consider the large solution  $u_-$ ,  $\nu_-$ , where  $s > 1$ . For such a solution, we have  $M = 0$  when  $\tau \ll 1$  and  $M = 2$  when  $\tau$  is sufficiently large. Moreover, there exists a*



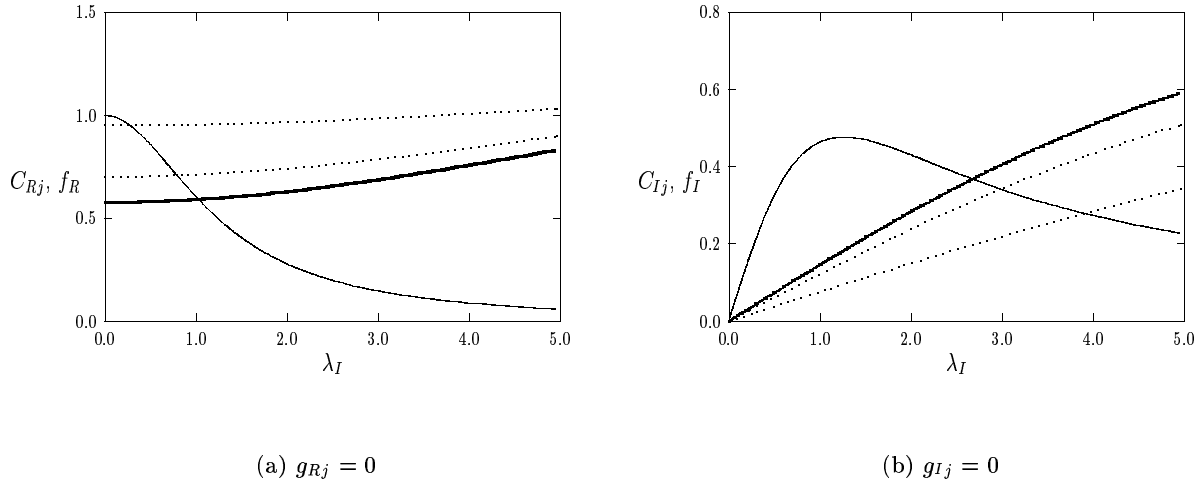


Figure 5: Parameter values are  $D = 0.75$ ,  $k = 3$ ,  $\mathcal{A} = 9.023$ , and  $\tau = 2.0$ . Left figure:  $C_{Rj}(\lambda_I)$ , for  $j = 1, \dots, 3$ , and  $f_R(\lambda_I)$  (solid curve). Right figure:  $C_{Ij}(\lambda_I)$  and  $f_I(\lambda_I)$  (solid curve). In these figures  $C_{R1}$  and  $C_{I1}$  are the heavy solid curves.

value  $\tau = \tau_{h1}$ , depending on  $\mathcal{A}$  and  $D$ , such that there is a pair of complex conjugate eigenvalues on the imaginary axis. For a multi-spike solution where  $k > 1$ , suppose that  $D < D_{kL}$  or  $\mathcal{A} > \mathcal{A}_{kL}$ . Then,  $M = 0$  when  $\tau \ll 1$  and  $M = 2k$  when  $\tau \gg 1$ . For  $k \geq 1$ , and for  $\tau$  sufficiently large, these eigenvalues are real and are on the interval  $0 < \lambda_R < \sigma_0 = 5/4$ . There are  $k$  eigenvalues  $\lambda_{Bj}$  that tend to  $\sigma_0 = 5/4$  from below as  $\tau \rightarrow \infty$ , and  $k$  eigenvalues  $\lambda_{Sj}$  that tend to zero as  $\tau \rightarrow \infty$ . The eigenvalues  $\lambda_{Bj}$  for  $j = 1, \dots, k$  have the common asymptotic behavior (3.31). In terms of the unique positive root  $\omega_j$  of  $C_j(\omega_j \tau^{-1}) = 1$ , the eigenvalues  $\lambda_{Sj}$  satisfy  $\lambda_{Sj} \sim \omega_j/\tau + O(\tau^{-2})$ , for  $j = 1, \dots, k$  and  $\tau \gg 1$ .

**Proof:** Let  $\tau > 0$ ,  $s > 1$ , and  $k \geq 1$ . Assume for  $k > 1$  that  $D < D_{kL}$ , or equivalently  $\mathcal{A} > \mathcal{A}_{kL}$ . We first show that  $M = 0$  when  $\tau \ll 1$  and  $M = 2k$  when  $\tau \gg 1$ . In this case, we have  $C_{Rj}(0) = B_j < f_R(0) = 1$  for  $j = 1, \dots, k$ , so that  $g_{Rj}(0) < 0$ . Therefore, by the monotonicity of  $g_{Rj}$ ,  $g_{Rj} = 0$  has a unique root for each  $j = 1, \dots, k$ . Moreover, since  $C_{Rj}(0) < 1$  it follows for  $\tau \ll 1$  that all of these roots must lie in some interval  $(0, \lambda_{Ic})$ , where  $\lambda_{Ic}$  is independent of  $\tau$ . Since  $C_{Ij} \rightarrow 0$  uniformly as  $\tau \rightarrow 0$  for any fixed  $\lambda_I$  from (3.28c), it follows for  $\tau \ll 1$  that  $g_{Ij} < 0$  whenever  $g_{Rj} = 0$ . Hence, for  $\tau \ll 1$  condition (1) in Proposition 3.9 applies. Therefore, from (3.29) we get  $M = 0$ . Alternatively, since at each fixed  $\lambda_I$ ,  $C_{Ij}$  increases without bound as  $\tau \rightarrow \infty$  from (3.28b), it follows that  $g_{Ij} > 0$  at the unique root of  $g_{Rj} = 0$ . Therefore, for  $\tau \gg 1$ , condition (2) in Proposition 3.9 holds, and we get  $M = 2k$  from (3.29). Next, we show that for  $k \geq 1$ , and  $\tau \gg 1$  that there are  $2k$  eigenvalues on the real axis in  $0 < \lambda_R < \sigma_0$ . Along the real axis, Proposition 3.5 shows that  $f(0) = 1$ , and  $f(\lambda_R)$  is an increasing, convex, function on  $0 < \lambda_R < \sigma_0$ . Moreover,  $f(\lambda_R) \rightarrow +\infty$  as  $\lambda_R \rightarrow \sigma_0^-$ , and  $f(\lambda_R) < 0$  for  $\lambda_R > \sigma_0$ . In contrast, from (3.19b) we have that  $C_j(\lambda_R)$  is a monotone increasing concave function, with an unbounded derivative for  $\tau \gg 1$ . When  $D < D_{kL}$ , or when  $\mathcal{A} > \mathcal{A}_{kL}$ , then  $C_j(0) = B_j < f(0) = 1$  for  $j = 1, \dots, k$ . Therefore, as  $\tau$  is increased, there exists a critical value  $\tau_{mj} > 0$  where  $C_j(\lambda_R)$  and  $f(\lambda_R)$  first intersect tangentially. For  $\tau > \tau_{mj}$  there

are two roots to  $g_j(\lambda) = 0$ . The values  $\tau = \tau_{mj}$  for  $j = 1, \dots, k$  are the values where complex conjugate eigenvalues merge onto the real axis. Clearly, as  $\tau \rightarrow \infty$ , one root of each  $g_j(\lambda_R) = 0$  tends to  $\sigma_0^-$  while the other root tends to zero. The precise asymptotic behavior of these roots as  $\tau \rightarrow \infty$  is obtained in a similar way as in Propositions 3.8 and 3.9 of [39]. Since for  $k = 1$ ,  $M = 0$  for  $\tau \ll 1$  and  $M = 2$  for  $\tau \gg 1$ , the existence of a Hopf bifurcation value  $\tau_{h1}$  (possibly non-unique) follows by continuity. ■

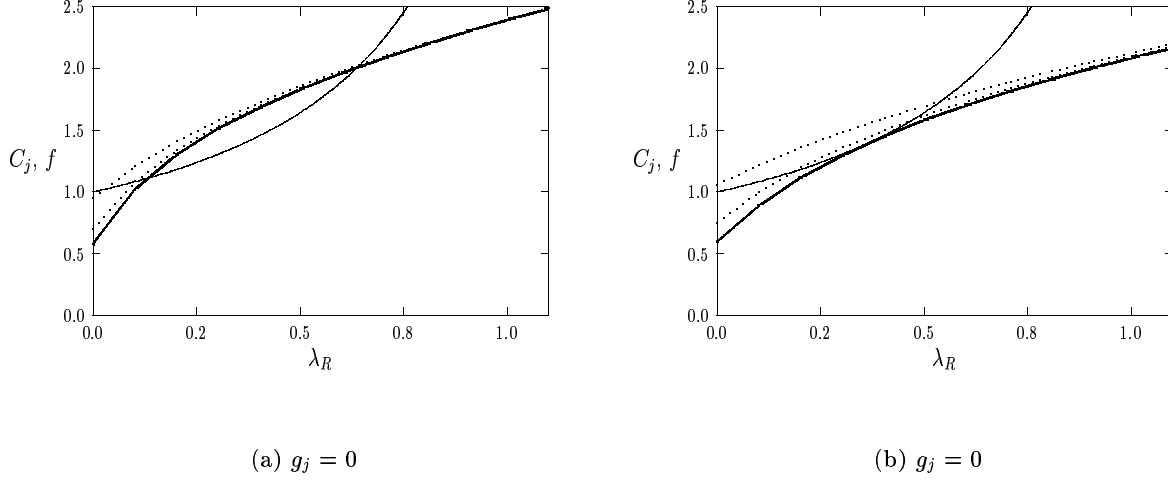


Figure 6: Plots of  $C_j(\lambda_R)$ , for  $j = 1$  (heavy solid curve) and  $j = 2, 3$  (dotted curves), with  $f_R(\lambda_R)$  (solid curve). Left figure: plots for  $D = 0.75$ ,  $k = 3$ ,  $\mathcal{A} = 9.023$ , and  $\tau = 80$ . Right figure: plots for  $D = 0.75$ ,  $k = 3$ ,  $\mathcal{A} = 8.357$ , and  $\tau = 36.93$ , where  $C_1(\lambda_R)$  intersects  $f(\lambda_R)$  tangentially. For this data  $\mathcal{A}_2 < \mathcal{A} < \mathcal{A}_{3L}$ .

We illustrate this result for  $D = 0.75$ ,  $k = 3$ ,  $\mathcal{A} = 9.023$ , and  $\tau = 2.0$ . For these values, Proposition 3.11 applies since, from (3.25b),  $\mathcal{A} > \mathcal{A}_{3L} = 8.686$ . In Fig. 5(a) and Fig. 5(b), we plot the numerically computed curves  $f_R(\lambda_I)$ ,  $C_{Rj}(\lambda_I)$  and  $f_I(\lambda_I)$ ,  $C_{Ij}(\lambda_I)$  for  $j = 1, \dots, 3$ . From these figures it follows that  $g_{Ij} < 0$  when  $g_{Rj} = 0$ . Therefore, since condition (1) of Proposition 3.9 holds for each  $j = 1, 2, 3$ , we get  $M = 0$  from (3.29). Hence, there are no eigenvalues of (3.11) in  $\text{Re}(\lambda) > 0$ . In Fig. 6(a) we plot  $C_j(\lambda_R)$  and  $f_R(\lambda_R)$  with  $\tau = 80$ , and for the same parameter values given above. For this larger value of  $\tau$ , each  $C_j(\lambda_R)$  intersects  $f_R(\lambda_R)$  exactly twice. Hence, there are six real positive eigenvalues on  $0 < \lambda_R < 5/4$ .

For a one-spike solution, the main limitation of Proposition 3.11 is that we cannot prove that the Hopf bifurcation value  $\tau_{h1}$  is unique. In particular, we cannot theoretically exclude the case that there are  $N$ , with  $N > 1$  and odd, values of  $\tau_{h1}$  where there are complex conjugate eigenvalues on the imaginary axis. To show that  $\tau_{h1}$  is unique one would have to prove a strict transversal crossing condition that states that whenever  $\tau > \tau_{h1}$  there must be exactly two eigenvalues in the right half-plane. From our numerical experiments in §3.3 and others not shown it appears that such a crossing condition does in fact hold. However, Proposition 3.11 does guarantee that there are two real positive eigenvalues for all  $\tau > \tau_{m1}$ .

For the large solution branch, the qualitative difference between the spectrum of (3.11) for a one-spike and for a multi-spike solution is that only for a multi-spike solution can eigenvalues cross through the

origin along the real axis  $\text{Im}(\lambda) = 0$  as  $D$  or  $\mathcal{A}$  is varied. However, when  $D < D_{kL}$  or  $\mathcal{A} > \mathcal{A}_{kL}$ , there are no real positive eigenvalues when  $\tau \ll 1$ . The real eigenvalues that exist when  $\tau \gg 1$  have occurred from the merging of complex conjugate pairs of eigenvalues onto the real axis. These complex conjugate eigenvalues arise from a Hopf bifurcation. Notice that since  $C_j(0)$  is independent of  $\tau$ , the eigenvalues of (3.11) can never cross through the origin along the real axis as  $\tau$  is increased. Therefore, instabilities as  $\tau$  is increased can only occur from Hopf bifurcations, whereas instabilities that occur as  $D$  is increased or  $\mathcal{A}$  is decreased occur from real eigenvalues entering the right half-plane.

The next result characterizes the number of eigenvalues in the right half-plane for a multi-spike solution for other ranges of  $D$  and  $\mathcal{A}$ , where there may be positive real eigenvalues when  $\tau \ll 1$ .

**Proposition 3.12:** *Let  $\tau > 0$ ,  $k > 1$ , and consider the multi-spike large solution  $u_-$ ,  $v_-$ , where  $s > 1$ . Suppose that there exists a  $j^*$  with  $2 \leq j^* \leq k$  such that either  $D_{j^*} < D < D_{j^*-1}$ , or  $\mathcal{A}_{j^*-1} < \mathcal{A} < \mathcal{A}_{j^*}$ . Here  $D_j$  and  $\mathcal{A}_j$  for  $j = 2, \dots, k$  are given in (3.22) and (3.23), respectively. Since there are no thresholds for  $j = 1$ , we conveniently label  $D_1 = \infty$  and  $\mathcal{A}_1 = \mathcal{A}_{1e}$ , where  $\mathcal{A}_{1e}$  is the existence threshold of (2.10). Then, for any  $\tau > 0$ , the number of eigenvalues  $M$  of (3.11) in the right half-plane satisfies the bounds*

$$1 + k - j^* \leq M \leq k - 1 + j^*. \quad (3.32)$$

Moreover, there are at least  $M_R = 1 + k - j^*$  positive real eigenvalues on  $0 < \lambda_R < 5/4$  for any  $\tau > 0$ .

**Proof:** The proof is simple. For the range of  $D$  and  $\mathcal{A}$  stated above, we have  $C_{Rj}(0) > 1$  for  $j = j^*, \dots, k$ , and  $C_{Rj}(0) < 1$  for  $j = 1, \dots, j^* - 1$ . Hence,  $g_{Rj}(\lambda_I) > 0$  for  $j = j^*, \dots, k$ , and condition (3) of Proposition 3.9 holds. This yields  $[\arg g_j]_{\Gamma_I} = -\pi/4$  for  $j = j^*, \dots, k$  and any  $\tau > 0$ . For the other indices, we proceed as in the proof of Proposition 3.11, to get  $[\arg g_j]_{\Gamma_I} = -5\pi/4$  for  $j = 1, \dots, j^* - 1$  when  $\tau$  is sufficiently small, and  $[\arg g_j]_{\Gamma_I} = 3\pi/4$  for  $j = 1, \dots, j^* - 1$  when  $\tau$  is sufficiently large. Substituting these values into the winding number criterion (3.29) we obtain (3.32). It is clear that there are at least  $M_R = 1 + k - j^*$  eigenvalues on the real axis when  $\tau \ll 1$ . This follows since  $C_j(0) = B_j > 1 = f(0)$  for  $j = j^*, \dots, k$ , and the fact that for any  $\tau > 0$  the curve  $C_j(\lambda_R)$  must intersect  $f(\lambda_R)$  exactly once for each  $j = j^*, \dots, k$ . ■

We illustrate this result for  $D = 0.75$ ,  $k = 3$ ,  $\mathcal{A} = 8.357$  and  $\tau = 36.93$ . For these values, (3.23) and (3.25b) yield  $\mathcal{A}_2 = 6.86$  and  $\mathcal{A}_{3L} = 8.686$ , so that  $\mathcal{A}_2 < \mathcal{A} < \mathcal{A}_{3L}$ . Therefore, we set  $j^* = k = 3$  in Proposition 3.12 to get  $1 \leq M \leq 5$ . In Fig. 6(b) we show the graphical determination of the eigenvalues of (3.11) on the positive real axis by plotting  $C_j(\lambda_R)$ , for  $j = 1, \dots, 3$ , and  $f(\lambda_R)$ . Since  $C_3(0) > 1$ , we only get one root of  $g_3 = 0$  for any  $\tau > 0$ . For the value  $\tau = 36.93$ , we have that  $C_1$  intersects  $f_R$  tangentially. For  $\tau \gg 1$ , it is clear that  $M = 5$ . For the smaller value  $\tau = 6.183$ , in Fig. 7(a) we plot  $f_R(\lambda_I)$  and  $C_{Rj}(\lambda_I)$  for  $j = 1, \dots, 3$ . A similar plot of  $f_I(\lambda_I)$  and  $C_{Ij}(\lambda_I)$ , for  $j = 1, \dots, 3$ , is shown in Fig. 7(b). For this value of  $\tau$ , we have  $g_{R1} = g_{I1} = 0$ . In addition, we have  $g_{I2} < 0$  when  $g_{R2} = 0$ , and that  $g_{R3}(\lambda_R) > 0$  for all  $\lambda_R > 0$ . Therefore, condition (1) and condition (3) of Proposition 3.9 holds for  $j = 2$  and  $j = 3$ , respectively. Then, from (3.29), it is clear that this value of  $\tau$  corresponds to where (3.11) has complex conjugate eigenvalues on the imaginary axis, together with one positive real eigenvalue.

**Remark 3.1:** As a special case of this result, we set  $j^* = 2$  to obtain  $k - 1 < M < k + 1$ . Therefore, when  $D > D_2$ , or when  $\mathcal{A} < \mathcal{A}_2$ , there are at least  $k - 1$  eigenvalues on the positive real axis. Here  $D_2$  and  $\mathcal{A}_2$  are given in (3.22) and (3.23), respectively. This range of the parameters is the near-shadow limit,

since we know that a  $k$ -spike solution for the shadow problem, obtained by letting  $D \rightarrow \infty$  in (1.5), will have  $k - 1$  eigenvalues on the positive real axis when  $\tau = 0$ . Hence, this qualitative feature of the spectrum is preserved for finite values of  $D$  up until  $D$  crosses below  $D_2$ . The  $k$ -spike hot-spot solution of the scalar nonlocal microwave heating model of [2], [3], and [13] has  $k - 1$  unstable real eigenvalues.

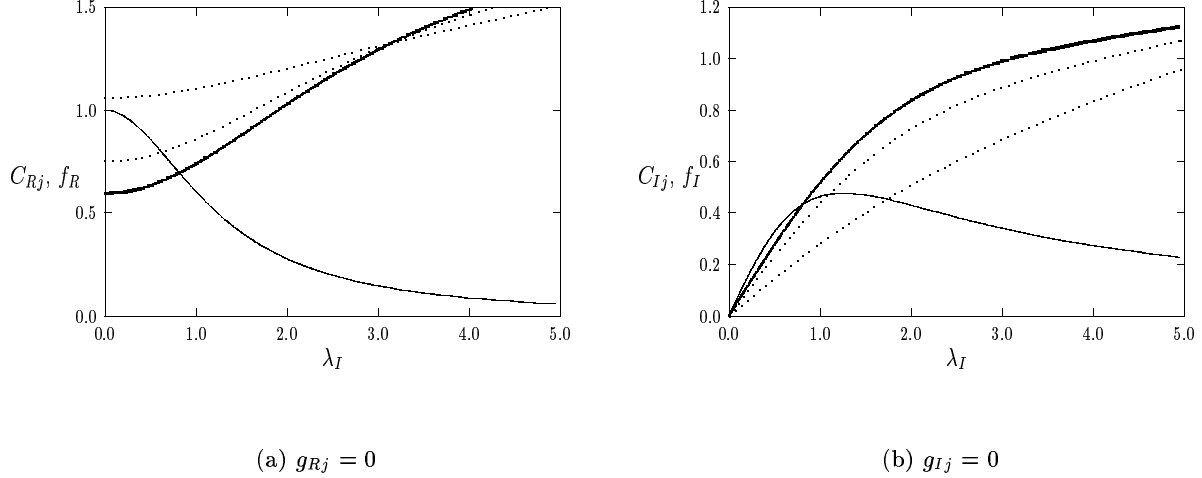


Figure 7: Parameter values  $D = 0.75$ ,  $k = 3$ ,  $\mathcal{A} = 8.357$ , and  $\tau = 6.183$ . Left figure:  $C_{Rj}(\lambda_I)$ , for  $j = 1, \dots, 3$ , and  $f_R(\lambda_I)$  (solid curve). Right figure:  $C_{Ij}(\lambda_I)$  and  $f_I(\lambda_I)$  (solid curve). In these figures  $C_{R1}$  and  $C_{I1}$  are the heavy solid curves.

The method of proof of Proposition 3.12 shows that there exists a value  $\tau = \tau_{hj} > 0$  (possibly non-unique) such that  $g_{Rj} = g_{Ij} = 0$ . At this value of  $\tau$ , there is a complex conjugate pair of eigenvalues on the imaginary axis. The minimum  $\tau_{hL}$  of these values determines the stability threshold. Therefore, we define

$$\tau_{hL} \equiv \text{Min}(\tau_{hj}; j = 1, \dots, k) . \quad (3.33)$$

The main stability results in this section can now be summarized succinctly as follows.

**Proposition 3.13:** *Let  $\tau > 0$ ,  $k > 1$ , and consider the multi-spike large solution  $u_-, \nu_-$ , where  $s > 1$ . For  $D < D_{kL}$ , or  $\mathcal{A} > \mathcal{A}_{kL}$ , the solution will be stable with respect to the large eigenvalues when  $0 < \tau < \tau_{hL}$ . Alternatively, suppose that  $D > D_{kL}$ , or  $\mathcal{A}_{ke} < \mathcal{A} < \mathcal{A}_{kL}$ , then the solution is unstable for any  $\tau > 0$ .*

Although we have not been able to prove a strict transversal crossing condition, all of the numerical experiments that we have performed indicate that the values  $\tau_{hj}$  are uniquely defined. Specifically, when  $\tau$  increases past a particular  $\tau_{hj}$  an additional pair of complex conjugate eigenvalues enters into the right half-plane and remains in this plane for all  $\tau > \tau_{hj}$ . Therefore, we conjecture that when  $D < D_{kL}$ , or when  $\mathcal{A} > \mathcal{A}_{kL}$ , the multi-spike solution will be unstable for any  $\tau$  with  $\tau > \tau_{hL}$ . When  $D > D_{kL}$ , or when  $\mathcal{A} < \mathcal{A}_{kL}$ , there is at least one positive real eigenvalue for any  $\tau > 0$ . In this range of  $D$  or  $\mathcal{A}$ , there may be additional complex conjugate pairs of eigenvalues in the right half-plane if  $\tau$  is large enough.

Next, we discuss the two types of instabilities that can occur for multi-spike solutions to (1.5). We first discuss **competition instabilities** that occur as a result of eigenvalues on the positive real axis. Suppose

that  $D$  satisfies  $D_{kL} < D < D_{k-1}$ , or equivalently  $\mathcal{A}_{k-1} < \mathcal{A} < \mathcal{A}_{kL}$ . Then, following the idea of the proof of Proposition 3.12, there will be exactly one eigenvalue in the right half-plane for  $0 < \tau < \tau_{hL}$ , and it is located along the real axis. Therefore, on this parameter range, the  $j = k$  mode governs the instability. The unstable eigenvalue,  $\lambda_{Rk} > 0$ , is the unique root of  $g_k(\lambda_R) = 0$ . From Principal Result 3.2, the unstable eigenvector is  $\mathbf{c}_k$  given in (3.10b). This implies that for some  $\delta \ll 1$  the initial instability of the large  $k$ -spike equilibrium solution has the form

$$\nu = \nu_- + \delta e^{\lambda_{Rk} t} \phi, \quad \phi(x) = \sum_{n=1}^k c_n \Phi[\varepsilon^{-1}(x - x_n)], \quad c_n = \cos\left(\frac{\pi(k-1)}{k}(n - 1/2)\right). \quad (3.34)$$

Since  $\sum_{n=1}^k c_n = 0$ , this instability locally preserves the sum of the heights of the spikes. Hence, we refer to it as a **competition instability**. As shown in the numerical experiments below in §3.3, this mode initiates a spike competition process, decreasing the amplitudes of some spikes while increasing the amplitudes of others. Numerically, it is found that this type of instability has the ultimate effect of annihilating spikes. A similar growing alternating-sign fluctuation of an activator-type variable was first observed in a different context in [16] and [15] (see Chapter 15 of [15]).

Next, we discuss the type of oscillatory instability that occurs when  $D < D_{kL}$ , or  $\mathcal{A} > \mathcal{A}_{kL}$ , as  $\tau$  increases past  $\tau_{hL}$ . The value of  $j$  for which the minimum in (3.33) is obtained determines the unstable eigenvector  $\mathbf{c}_j$  in Principal Result 3.2. We now develop a criterion to determine which mode goes unstable first as  $\tau$  is increased. To do so, we first try to develop an ordering principle for  $C_{Rj}$  and  $C_{Ij}$ . From (3.17) and (3.26c), we obtain for  $j = 1, \dots, k-1$  that

$$C_{Rj+1} - C_{Rj} = \beta_j \operatorname{Re}[E(\xi)], \quad C_{Ij+1} - C_{Ij} = \beta_j \operatorname{Im}[E(\xi)], \quad E(\xi) \equiv \frac{\xi}{\sinh \xi}. \quad (3.35a)$$

Here  $\beta_j > 0$  and the complex variable  $\xi$  are defined by

$$\beta_j \equiv \left(\frac{k}{2\theta_0 s}\right) \left(\frac{\sin[\pi(j-1/2)/k] \sin[\pi/(2k)]}{\tanh(\theta_0/k)}\right) > 0, \quad \xi \equiv \frac{2\theta_0}{k} \sqrt{1 + i\tau\lambda_I}. \quad (3.35b)$$

This leads to the following ordering principle:

**Lemma 3.14:** *Suppose that  $\operatorname{Re}[E(\xi)] > 0$  and  $\operatorname{Im}[E(\xi)] < 0$  at each point on some interval  $0 < \lambda_I < \lambda_*$ . Then, we have the following ordering principle on  $0 < \lambda_I < \lambda_*$ :*

$$C_{R1}(\lambda_I) < \dots < C_{Rk}(\lambda_I), \quad C_{I1}(\lambda_I) > \dots > C_{Ik}(\lambda_I). \quad (3.36)$$

When this principle holds,  $j = 1$  is the first unstable mode. We state the result as follows.

**Proposition 3.15:** *Let  $\varepsilon \rightarrow 0$ ,  $k > 1$ , and consider the large solution  $u_-$ ,  $\nu_-$ . Let  $\tau = \tau_{h1}$  and  $\lambda_I = \lambda_{h1}$  correspond to the minimum value of  $\tau$  for which  $g_{R1} = g_{I1} = 0$  has a root. Suppose that for  $\tau = \tau_{h1}$ , the ordering principle of Lemma 3.14 holds at each point on the interval  $0 < \lambda_I < \lambda_{h1}$ . Then, there are either zero or two eigenvalues in  $\operatorname{Re}(\lambda) > 0$  for  $\tau$  in a small neighborhood of  $\tau = \tau_{h1}$ .*

**Proof:** Since the ordering principle (3.36) holds when  $\tau = \tau_{h1}$ , it follows by continuity that it holds in a sufficiently small neighborhood of  $\tau_{h1}$ . Therefore, we will have  $g_{Ij} < 0$  whenever  $g_{Rj} = 0$  for  $j = 2, \dots, k-1$ .

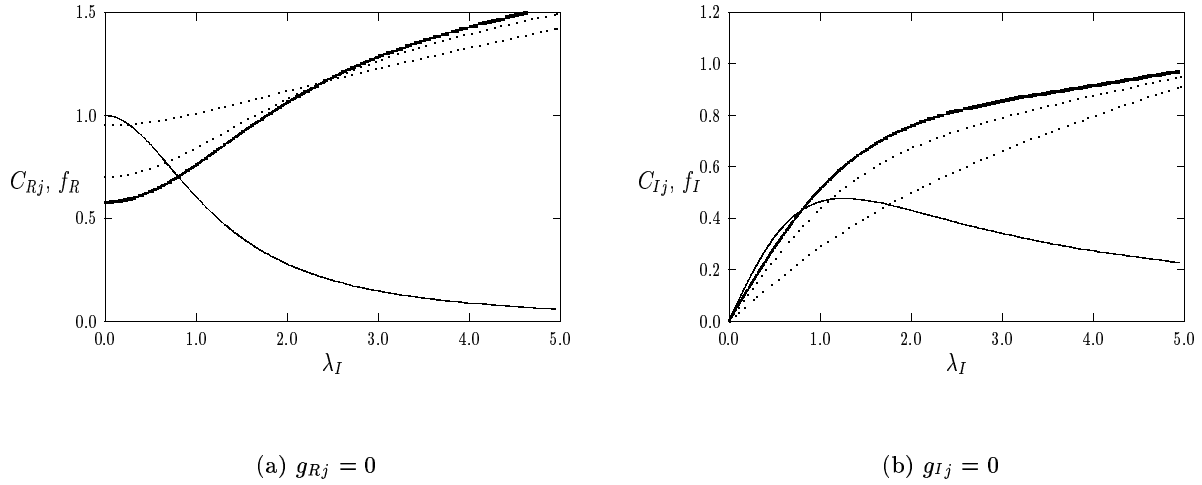


Figure 8: Parameter values  $D = 0.75$ ,  $k = 3$ ,  $\mathcal{A} = 9.023$ , and  $\tau = 8.049$ . Left figure:  $C_{Rj}(\lambda_I)$ , for  $j = 1, \dots, 3$ , and  $f_R(\lambda_I)$  (solid curve). Right figure:  $C_{Ij}(\lambda_I)$  and  $f_I(\lambda_I)$  (solid curve). In these figures  $C_{R1}$  and  $C_{I1}$  are the heavy solid curves.

This implies that condition (1) of Proposition 3.9 holds, and so we get  $[\arg g_j]_{\Gamma_I} = -5\pi/4$  for  $j = 2, \dots, k$ . From (3.29) we get  $M = 0$  or  $M = 2$  depending on whether  $[\arg g_1]_{\Gamma_I} = -5\pi/4$  or  $[\arg g_1]_{\Gamma_I} = 3\pi/4$ . ■

To illustrate this result we choose the parameters  $D = 0.75$ ,  $k = 3$ , and  $\mathcal{A} = 9.023 > \mathcal{A}_{3L}$ , of Fig. 5. For  $\tau = 8.049$ , in Fig. 8(a) we plot the numerically computed  $f_R(\lambda_I)$  and  $C_{Rj}(\lambda_I)$  for  $j = 1, \dots, 3$ . In Fig. 8(b) we plot  $f_I(\lambda_I)$  and  $C_{Ij}(\lambda_I)$ , for  $j = 1, \dots, 3$ . For this value of  $\tau$  it is clear from these figures that the ordering principle (3.36) holds, and so  $j = 1$  sets the stability threshold. Therefore, for  $\tau = 8.049$ , it follows that (3.11) has no eigenvalues in the right half-plane, but has a pair of complex conjugate eigenvalues on the imaginary axis determined by the  $j = 1$  mode. This is the Hopf bifurcation value.

Under the conditions of Proposition 3.15,  $j = 1$  is the first unstable mode. The corresponding eigenvector from (3.10b) is  $\mathbf{c}_1^t = (1, \dots, 1)$ . Thus, for  $\tau = \tau_{h1}$  the initial instability of the large solution is

$$\nu = \nu_- + \delta e^{i\lambda_{h1}t} \phi + \text{c.c.}, \quad \phi(x) = \sum_{n=1}^k c_n \Phi[\varepsilon^{-1}(x - x_n)], \quad c_n = 1, \quad n = 1, \dots, k. \quad (3.37)$$

Here c.c. denotes complex conjugate,  $\delta \ll 1$ , and  $\lambda_{h1}$  is the root of  $g_{R1} = g_{I1} = 0$ , which occurs when  $\tau = \tau_{h1}$ . The key observation is that since  $c_n = 1$ , for  $n = 1, \dots, k$ , the initial form of the instability is to synchronize the amplitudes of the spikes. We refer to this as a **synchronous oscillatory instability**. Therefore, if the ordering principle in Lemma 3.14 holds, the  $j = 1$  mode goes unstable first, and the effect is to synchronize the small-scale oscillations in the spike amplitudes.

The critical condition in Lemma 3.14 is to determine the signs of  $\text{Re}[E(\xi)]$  and  $\text{Im}[E(\xi)]$ . Writing  $\xi = \xi_R + i\xi_I$ , a simple calculation shows that  $\text{Re}[E(\xi)] > 0$  and  $\text{Im}[E(\xi)] < 0$  if and only if

$$\tanh \xi_R \cos \xi_I + \frac{\xi_I}{\xi_R} \sin \xi_I > 0, \quad \text{and} \quad \sin \xi_I - \frac{\xi_I}{\xi_R} \tanh \xi_R \cos \xi_I > 0. \quad (3.38)$$

From the definition of  $\xi$  in (3.35b), it follows that (3.38) holds when  $\tau\lambda_I$  is small enough. Therefore, it is natural to look for a condition where the  $j = 1$  sets the stability threshold.

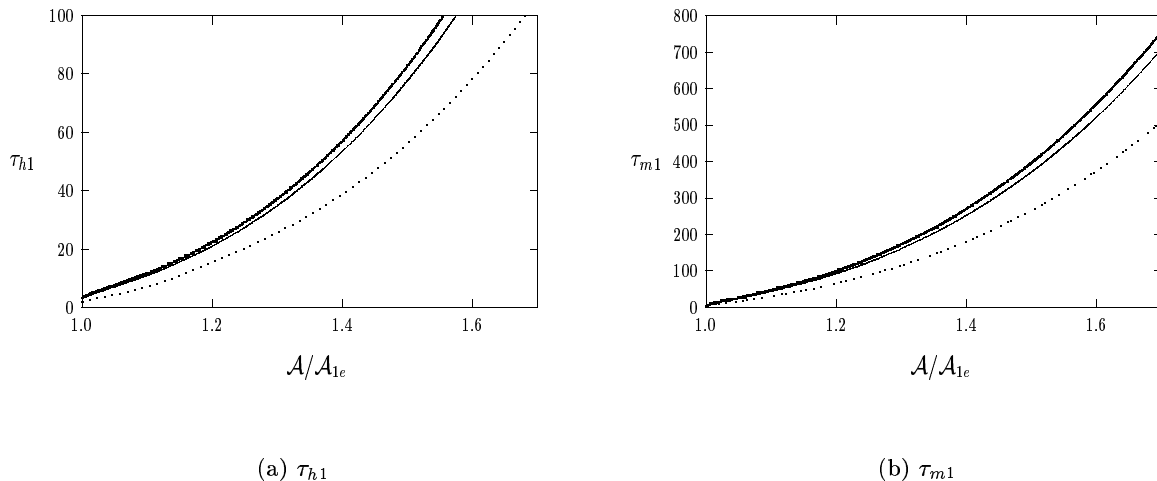


Figure 9: Left figure: the Hopf bifurcation value  $\tau_{h1}$  versus  $\mathcal{A}/\mathcal{A}_{1e}$  for a one-spike solution. Right figure:  $\tau_{m1}$  versus  $\mathcal{A}/\mathcal{A}_{1e}$  where the complex pair of eigenvalues merge onto the positive real axis. The labels are  $D = 0.75$  (dashed curve),  $D = 0.25$  (solid curve), and  $D = 0.1$  (heavy solid curve).

Finally, we remark on the possibility of asynchronous small-scale oscillation near the Hopf bifurcation point  $\tau_{hL}$ . Such an instability is governed by the  $j = k$  mode which, as discussed with respect to competition instabilities, has the effect of locally conserving the spike amplitudes. The  $j = k$  mode sets the initial instability when both  $\text{Re}[E(\xi)]$  and  $\text{Im}[E(\xi)]$  have exactly one zero-crossing on the interval  $0 < \lambda_I < \lambda_{hk}$ , where  $\lambda_I = \lambda_{hk}$  and  $\tau = \tau_{hk}$  is the root of  $g_{Rk} = g_{Ik} = 0$ . Although we show in Example 4 of §3.3 that asynchronous oscillatory instabilities are theoretically possible in a narrow parameter range, we have not been able to numerically observe such oscillations in the GS model (1.5) in the low feed-rate regime.

### 3.3 Numerical Results: Oscillatory and Competition Instabilities

We now give some numerical results for the stability thresholds studied rigorously in §3.2. Here we will only consider instabilities of the large solution. To illustrate our results we take  $D = 0.75$  and  $D = 0.1$ . For  $D = 0.75$ , the spike interaction is strong and oscillatory instabilities occur for small values of  $\tau$ . Moreover, spike competition instabilities due to positive real eigenvalues can also occur far from the existence threshold  $\mathcal{A}_{ke}$ . Alternatively, for  $D = 0.1$ , the inter-spike interaction is relatively weak and the finite domain does not play a very significant role in generating instabilities, unless there are many spikes. More specifically, for  $k\sqrt{D} \ll 1$ , instabilities due to positive real eigenvalues only occur very close to the existence threshold  $\mathcal{A}_{ke}$ . Recall also from (1.3), that our formulation of the GS model required that  $\tau > 1$ . All of the stability thresholds for a Hopf bifurcation computed below for  $D = 0.75$  and  $D = 0.1$  satisfy this condition.

For  $k = 1$ , in Fig. 9(a) we plot the Hopf bifurcation threshold  $\tau_{h1}$  versus  $\mathcal{A}/\mathcal{A}_{1e}$  for  $D = 0.75$ ,  $D = 0.25$ , and  $D = 0.1$ . These results suggest that  $\tau_{h1}$  is an increasing function of  $\mathcal{A}/\mathcal{A}_{1e}$ , and that the stability

threshold  $\tau_{h1}$  is larger for smaller values of  $D$ . This is intuitive since for smaller values of  $D$  the interaction of the spike with the boundaries of the domain is weaker. In Fig. 9(b) we plot the values  $\tau_{m1}$  where complex conjugate eigenvalues first merge onto the real axis. In Fig. 10(a) we plot the Hopf bifurcation frequency  $\lambda_{h1}$  versus  $\mathcal{A}/\mathcal{A}_{1e}$ . This frequency tends to a limiting value  $\lambda_{h1} \approx 0.53$  for  $\mathcal{A}/\mathcal{A}_{1e} \gg 1$  (see §4).

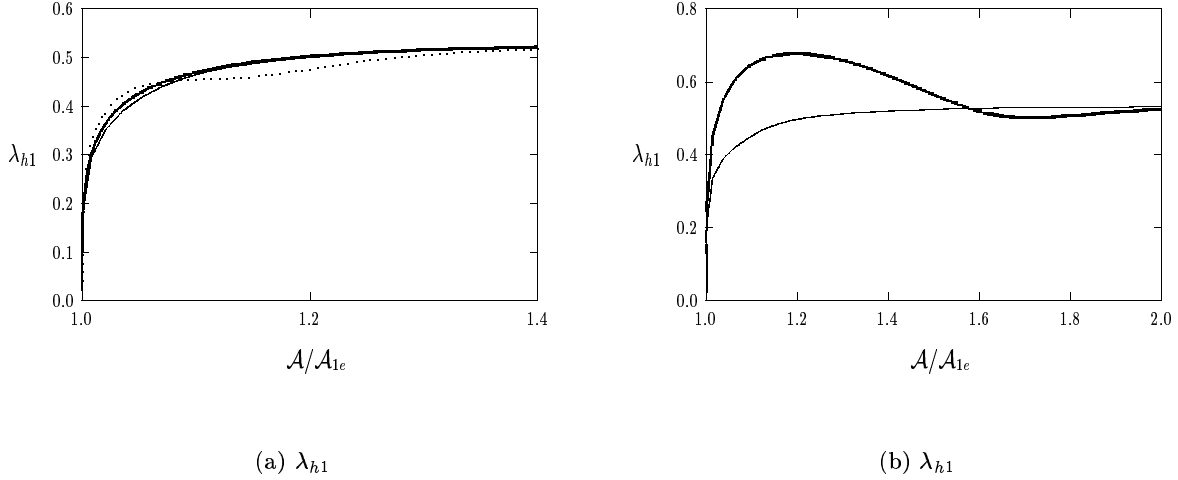


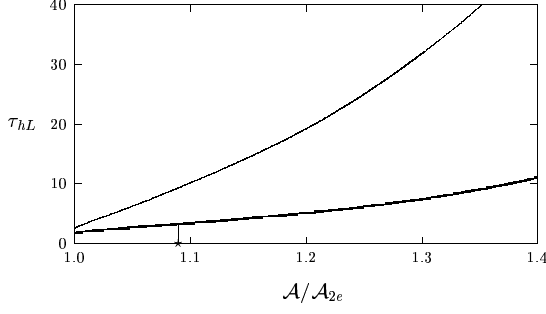
Figure 10: Left figure: the Hopf bifurcation frequency  $\lambda_{h1}$  versus  $\mathcal{A}/\mathcal{A}_{1e}$  for a one-spike solution with  $D = 0.75$  (dashed curve),  $D = 0.25$  (solid curve), and  $D = 0.1$  (heavy solid curve). Right figure  $\lambda_{h1}$  for a two-spike solution with  $D = 0.75$  (heavy solid curve) and  $D = 0.1$  (solid curve).

Next we consider two-spike solutions for  $D = 0.75$  and  $D = 0.1$ . From (2.10) and (3.25b), we calculate the critical values  $\mathcal{A}_{2e}$  and  $\mathcal{A}_{2L}$  as

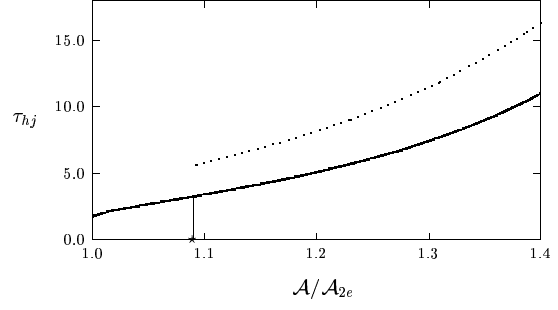
$$\mathcal{A}_{2e} = 5.158, \quad \mathcal{A}_{2L} = 5.633, \quad \text{for } D = 0.75; \quad \mathcal{A}_{2e} = 6.427, \quad \mathcal{A}_{2L} = 6.433, \quad \text{for } D = 0.1. \quad (3.39)$$

In Fig. 11(a) we plot the Hopf bifurcation value  $\tau_{hL}$  as a function of  $\mathcal{A}/\mathcal{A}_{2e}$  for both values of  $D$ . This threshold is set by the  $j = 1$  mode. In this diagram we have indicated, by a vertical line, the value  $\mathcal{A}_{2L}/\mathcal{A}_{2e}$ . Recall that below this value there are eigenvalues on the positive real axis for any  $\tau > 0$ . Since  $\mathcal{A}_{2L}$  is very close to  $\mathcal{A}_{2e}$  when  $D = 0.1$ , a competition instability for this value of  $D$  occurs only in a narrow parameter regime. The corresponding frequency  $\lambda_{h1}$  is plotted in Fig. 10(b). In Fig. 11(b) we plot a more detailed stability threshold for  $D = 0.75$ . In this plot we have indicated by a dashed line the threshold  $\tau_{h2}$  at which an additional pair of complex conjugate eigenvalues enter the right half-plane. Hence, for  $\mathcal{A} > \mathcal{A}_{2L}$  and  $\tau > \tau_{h2}$  there are four eigenvalues in the right half-plane. From the theory developed earlier, the curve  $\tau_{h2}$  versus  $\mathcal{A}/\mathcal{A}_{2e}$  terminates when  $\mathcal{A} \rightarrow \mathcal{A}_{2L}^+$  since the complex conjugate pair for the  $j = 2$  mode coalesce at the origin  $\lambda = 0$ . One eigenvalue then moves along the positive real axis, while the other moves along the negative real axis as  $\mathcal{A}$  is decreased below  $\mathcal{A}_{2L}$ .

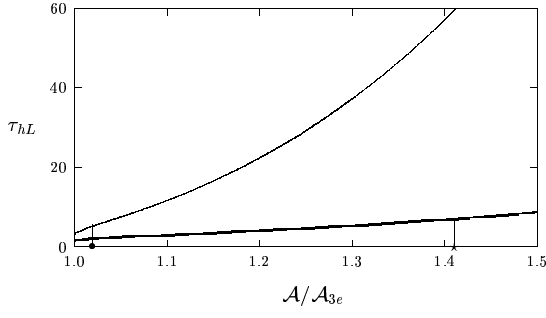




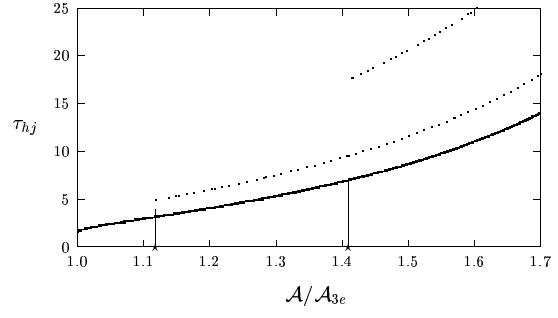
(a)  $\tau_{hL}$ ,  $k = 2$



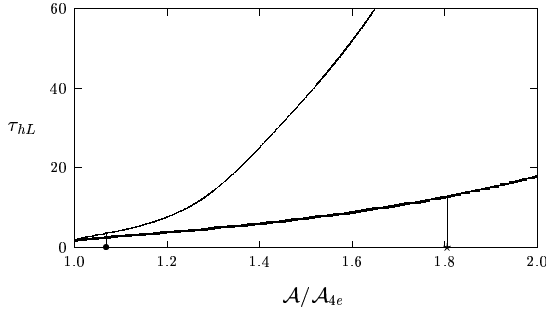
(b)  $\tau_{hj}$ ,  $k = 2$



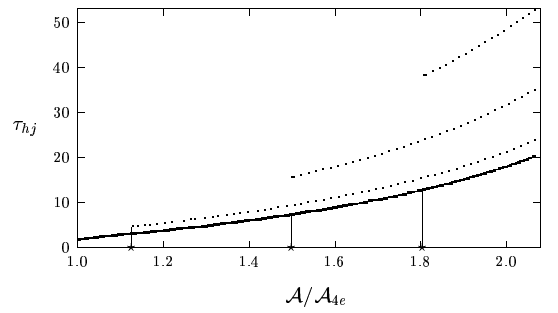
(c)  $\tau_{hL}$ ,  $k = 3$



(d)  $\tau_{hj}$ ,  $k = 3$



(e)  $\tau_{hL}$ ,  $k = 4$



(f)  $\tau_{hj}$ ,  $k = 4$

Figure 11: The Hopf bifurcation value  $\tau_{hL}$  versus  $\mathcal{A}/\mathcal{A}_{ke}$  for  $k = 2$  (top row),  $k = 3$  (middle row), and  $k = 4$  (bottom row). In the left figures we plot  $\tau_{hL}$  for  $D = 0.75$  (heavy solid curves) and  $D = 0.1$  (solid curves). For  $D = 0.75$ , in the right figures we plot  $\tau_{hL}$  (heavy solid curve) and  $\tau_{hj}$  (dashed curves) for  $j = 2, \dots, k$ .

For three-spike solutions with  $D = 0.75$  and  $D = 0.1$ , we get from (2.10), (3.23), and (3.25b), that

$$\mathcal{A}_{3e} = 6.145, \quad \mathcal{A}_2 = 6.864, \quad \mathcal{A}_{3L} = 8.6857, \quad \text{for } D = 0.75, \quad (3.40a)$$

$$\mathcal{A}_{3e} = 6.960, \quad \mathcal{A}_2 = 6.978, \quad \mathcal{A}_{3L} = 7.0904, \quad \text{for } D = 0.1. \quad (3.40b)$$

Similarly, for four-spike solutions we obtain the thresholds

$$\mathcal{A}_{4e} = 7.023, \quad \mathcal{A}_2 = 7.914, \quad \mathcal{A}_3 = 10.52, \quad \mathcal{A}_{4L} = 12.69, \quad \text{for } D = 0.75, \quad (3.41a)$$

$$\mathcal{A}_{4e} = 7.589, \quad \mathcal{A}_2 = 7.619, \quad \mathcal{A}_3 = 7.830, \quad \mathcal{A}_{4L} = 8.127, \quad \text{for } D = 0.1. \quad (3.41b)$$

In Fig. 11(c) and Fig. 11(e) we plot  $\tau_{hL}$  versus  $\mathcal{A}/\mathcal{A}_{ke}$  for three and four-spike solutions when  $D = 0.75$  and  $D = 0.1$ . For the larger value  $D = 0.75$ , in Fig. 11(d) and Fig. 11(f) we show the detailed stability diagram by plotting  $\tau_{hj}$  for  $j = 2, \dots, k$ . In each case, the stability threshold  $\tau_{hL}$  is set by the  $j = 1$  mode representing synchronous oscillations. The vertical lines in these figures indicate where positive real eigenvalues enter the right half-plane. The information in Proposition 3.12 is succinctly contained in these detailed stability diagrams. For instance, from Fig. 11(f) for  $D = 0.75$ , we see that if  $\mathcal{A}$  satisfies  $7.914 < \mathcal{A} < 10.52$ , then there are two real eigenvalues in the right half-plane when  $\tau < \tau_{hL}$  and six eigenvalues (at least two real) in the right half-plane when  $\tau > \tau_{h2}$ .

We now consider some specific examples of the theory, and we compare the results with full-scale numerical simulations of (1.5). The solution to (1.5) is computed using the routine D03PCF of the NAG library [27] with 1500 uniformly spaced meshpoints. In terms of the  $k$ -spike equilibrium solution of Principal Result 2.1, in each of the experiments below the initial condition for (1.5) is taken to be

$$\nu(x, 0) = \nu_-(x) \left[ 1 + 0.01 \sum_{j=1}^k (-1)^{j+1} \cos \left( \frac{\pi(x - x_j)}{\varepsilon} \right) e^{-(x-x_j)^2/(2\varepsilon^2)} \right], \quad u(x, 0) = u_-(x). \quad (3.42)$$

**Example 1:** We first consider a one-spike solution to (1.5) for  $D = 0.75$ ,  $\mathcal{A} = 4.563$ , and  $\varepsilon = 0.01$ . In Fig. 12(a) we plot the spike amplitude  $\nu_m \equiv \nu(0, t)$  for two values of  $\tau$ . From this figure, we observe decaying and growing spike oscillations when  $\tau = 7.5$  and  $\tau = 7.8$ , respectively. From the data used to generate Fig. 9(a), the Hopf bifurcation value is  $\tau_{hL} \approx 7.7$ . In Fig. 12(b) we plot the spike amplitude  $\nu_m$  versus  $t$  for two values of  $\tau$  when  $D = 0.1$ ,  $\mathcal{A} = 6.59$ , and  $\varepsilon = 0.01$ . The spike oscillations are found to decay when  $\tau = 8.6$  and grow when  $\tau = 8.8$ . The Hopf bifurcation value from Fig. 9(a) is  $\tau_{hL} \approx 8.7$ . Although our theory correctly predicts the Hopf bifurcation value, it does not explain the large-scale oscillations seen in Fig. 12(b) whereby the instability ultimately leads to the annihilation of the spike.

**Example 2:** Next, we consider a three-spike solution to (1.5) with  $D = 0.75$  and  $\varepsilon = 0.1$ . We first take the parameter values  $\mathcal{A} = 8.6$  and  $\tau = 2.0$ . Since  $\mathcal{A}$  satisfies  $\mathcal{A}_2 < \mathcal{A} < \mathcal{A}_{3L}$  from (3.40a), and  $\tau$  is below the Hopf bifurcation value, we expect a competition instability. In Fig. 13(a) we plot the initial condition (3.42) used for the numerical solution of (1.5). In Fig. 13(b) we show the competition instability that occurs from the unique real positive eigenvalue in the right half-plane. Although we can correctly predict the onset of the competition instability, the nonlinear mechanisms leading to the annihilation of the second spike as seen in Fig. 13(b) is an open problem. Next, we take the slightly larger value  $\mathcal{A} = 8.86$ , so that

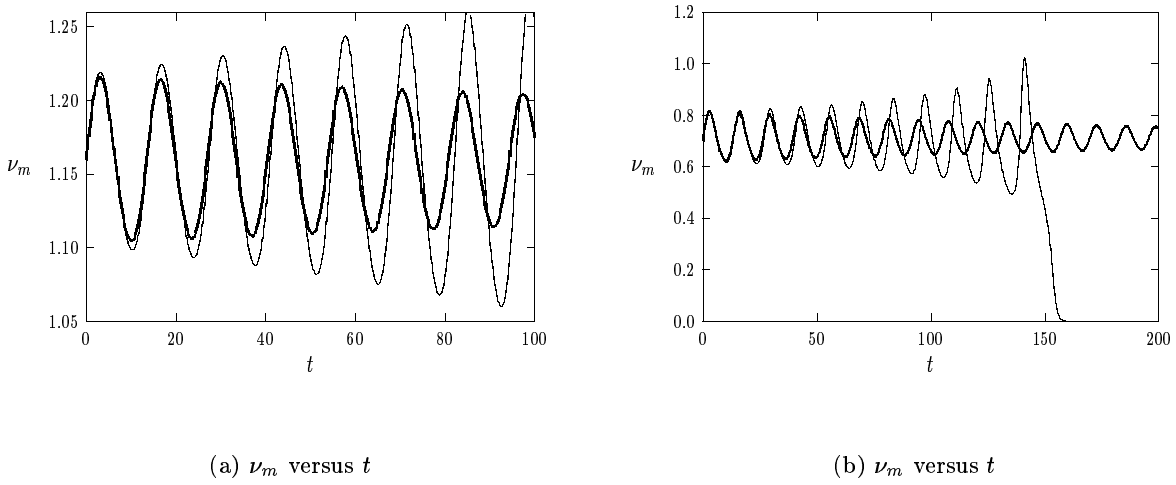


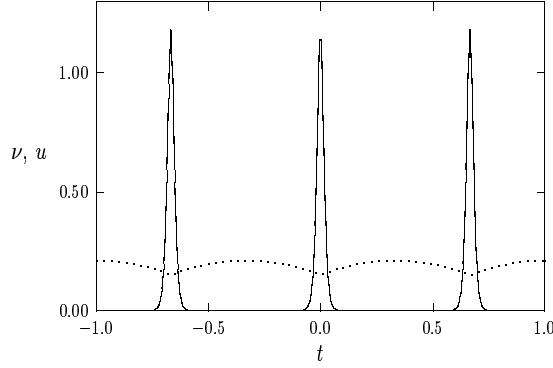
Figure 12: Example 1: Plots of  $\nu_m$  versus  $t$  for  $k = 1$  with  $\varepsilon = 0.01$ . Left figure:  $D = 0.75$  and  $\mathcal{A} = 4.563$ , with  $\tau = 7.5$  (heavy solid curve) and  $\tau = 7.8$  (solid curve). Right figure:  $D = 0.1$  and  $\mathcal{A} = 6.59$ , with  $\tau = 8.6$  (heavy solid curve) and  $\tau = 8.8$  (solid curve).

now  $\mathcal{A} > \mathcal{A}_{3L} = 8.6857$ . For this value, the data used to generate Fig. 11(c) yields the Hopf bifurcation value  $\tau_{hL} \approx 7.5$ . For  $\tau = 7.25$ , in Fig. 14(a) we show a synchronous decaying oscillation in the spike amplitudes. For the slightly larger value  $\tau = 7.6$ , in Fig. 14(b) we show both the onset of a synchronous oscillatory instability, and the ultimate simultaneous annihilation of the three spikes.

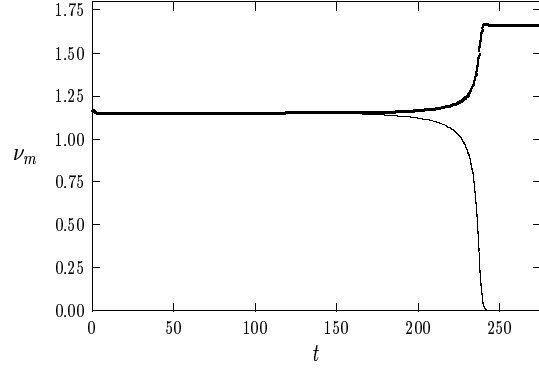
**Example 3:** This is the four-spike example for  $D = 0.1$  and  $\varepsilon = 0.01$  shown in Fig. 2 and Fig. 3 of §1. Since  $\mathcal{A}_3 = 7.83$  and  $\mathcal{A}_{4L} = 8.127$  from (3.41b), there is a competition instability when  $\mathcal{A} = 8.0$  and  $\tau$  is below the Hopf bifurcation value. This is clearly observed in Fig. 2(b) where  $\tau = 2.0$ . For this value of  $\mathcal{A}$ , from the data used to generate Fig. 11(e), there is a Hopf bifurcation when  $\tau \approx 3.4$ . For this value of  $\tau$  there is a pair of complex conjugate eigenvalues on the imaginary axis, together with a positive real eigenvalue. Therefore, for  $\tau = 3.2$ , the initial instability should be a superposition of a competition instability and a synchronous decaying oscillation in the spike amplitudes. This is shown in Fig. 15. These two types of instabilities lead to an initial synchronization of the spike oscillations, followed by a spike competition.

Alternatively, suppose that we take the larger value  $\mathcal{A} = 8.3 > \mathcal{A}_{4L}$ . From the data used to plot Fig. 11(e) we obtain that the Hopf bifurcation now occurs when  $\tau \approx 4.0$ . In Fig. 3(a) of §1 we showed a synchronous decaying oscillation in the spike amplitudes when  $\tau = 3.8$ . For  $\tau = 4.1$ , Fig. 3(b) of §1 shows a synchronous oscillatory instability in the spike amplitudes followed by a simultaneous spike annihilation. Since  $D = 0.1$  is small for this example, we might naively expect that the inter-spike interaction is very weak. However, for four spikes, the interaction is sufficiently strong so that these instabilities occur rather far from the existence threshold  $\mathcal{A}_{4e} = 7.589$ .

**Example 4:** In this example we try to determine asynchronous oscillations of a two-spike solution. We let  $D = 0.25$  and we compute the critical values  $\tau_{h1}$  and  $\tau_{h2}$  versus  $\mathcal{A}/\mathcal{A}_{2e}$  where complex conjugate pairs of eigenvalues enter the right half-plane. The plot is shown in Fig. 16(a). The Hopf bifurcation value  $\tau_{hL}$  is the

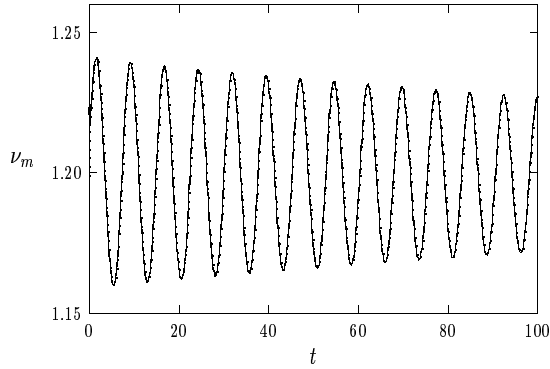


(a) The initial condition

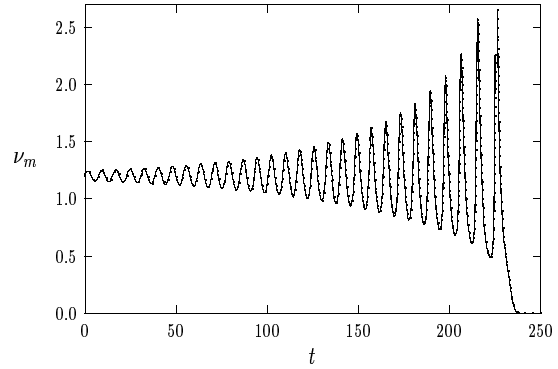


(b)  $\nu_m$  versus  $t$

Figure 13: Example 2: Here  $k = 3$ ,  $D = 0.75$ ,  $\mathcal{A} = 8.6$ ,  $\varepsilon = 0.01$ , and  $\tau = 2.0$ . Left figure: the initial condition for  $\nu$  (solid curve) and  $u$  (dashed curve). Right figure: The spike amplitudes  $\nu_m$ . The middle spike is annihilated, and the other two spikes have a common amplitude.



(a)  $\nu_m$  versus  $t$



(b)  $\nu_m$  versus  $t$

Figure 14: Example 2: The parameters are  $k = 3$ ,  $D = 0.75$ ,  $\mathcal{A} = 8.86$ , and  $\varepsilon = 0.01$ . Left figure: synchronous decaying amplitude oscillations for  $\tau = 7.25$ . Right figure: synchronous oscillatory instability for  $\tau = 7.6$ , leading to a simultaneous collapse. The spike amplitudes trace out identical trajectories.

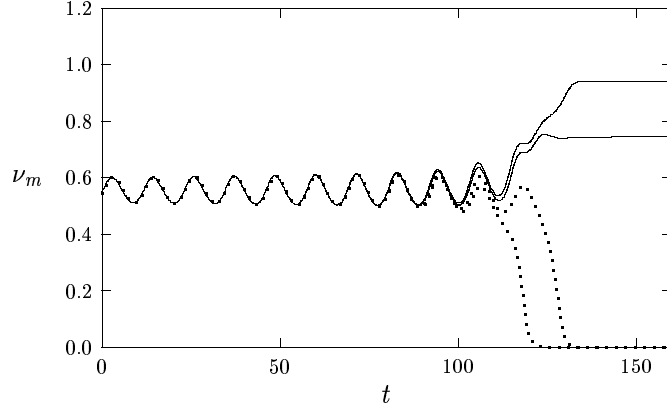


Figure 15: Example 3: The parameters are  $k = 4$ ,  $D = 0.1$ ,  $\varepsilon = 0.01$ ,  $\mathcal{A} = 8.0$  and  $\tau = 3.2$ . Synchronized oscillations of the spike amplitudes are followed by a competition leading to the annihilation of the second spike and then the fourth spike. Of the two remaining spikes, the third has the largest amplitude.

minimum of these two values. From this figure we notice that the two curves  $\tau_{h1}$  and  $\tau_{h2}$  cross exactly once at some value of  $\mathcal{A}/\mathcal{A}_{2e}$ , and that they both asymptote to a common limiting behavior as  $\mathcal{A}/\mathcal{A}_{2e} \rightarrow \infty$ . This limiting behavior is analyzed in §5 when we study the intermediate regime. On the range where  $\tau_{h1} < \tau_{h2}$  in Fig. 16(a) we expect synchronous oscillations as  $\tau$  is increased beyond  $\tau_{h1}$ . Asynchronous oscillations should occur on the narrow range where  $\tau_{h2} < \tau_{h1}$  as  $\tau$  is increased. As a remark, when  $D = 0.25$  we compute that  $\mathcal{A}_{2e} = 5.614$  and  $\mathcal{A}_{2L} = 5.681$ . Hence, there will be no competition instabilities due to real eigenvalues crossing into the right half-plane when  $\mathcal{A} > 5.681$ .

To illustrate the resulting spike dynamics we take  $\mathcal{A} = 7.9377$  and  $\varepsilon = 0.01$ . We compute that  $\tau_{h1} = 36.1$  and  $\tau_{h2} = 35.6$ . Hence, the complex eigenvalues that first enter the right half-plane as  $\tau$  is increased corresponds to the asynchronous mode. In Fig. 16(b) we plot the numerically computed spike amplitudes for three values of  $\tau$  starting from the asynchronous initial condition (3.42). For each of these values of  $\tau$ , the spike amplitudes are found to synchronize very quickly in time. For  $\tau = 40$ , the spike amplitudes both collapse, for  $\tau = 34$  they exhibit a large-scale periodic oscillation, and for  $\tau = 30$  the oscillations relax back to the equilibrium state as  $t$  increases. We have done many other examples to try to determine asynchronous oscillations in the low feed-rate regime without success. However, asynchronous oscillations for the spike amplitudes have been observed in the pulse-splitting parameter regime where  $\mathcal{A} = O(\varepsilon^{-1/2})$ , or equivalently where  $A = O(1)$  (see [17]). There are two possibilities for not observing such oscillations in the low feed-rate regime. One possibility is that the asynchronous mode is unstable in the weakly nonlinear regime. The second possibility results from our observation that whenever  $\tau_{hL} = \tau_{hk}$ , so that stability is set by the asynchronous mode, the threshold for the synchronous mode  $\tau_{h1}$  has a numerical value that is typically very close to  $\tau_{hk}$ . Hence, whenever asynchronous oscillations are theoretically possible as  $\tau$  is increased, we have typically found that the more dominant synchronous mode is essentially also present.

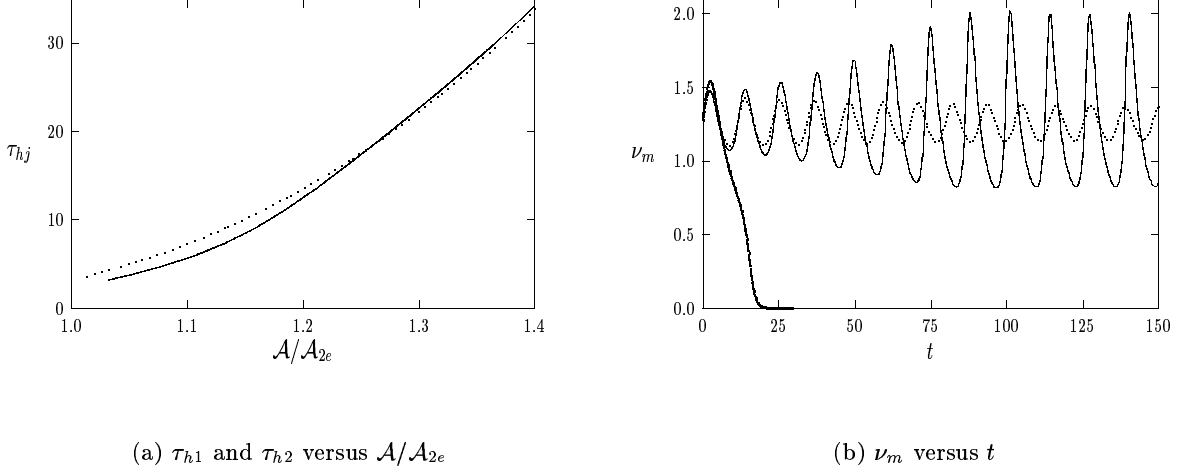


Figure 16: Example 4: Left figure: The critical values  $\tau_{h1}$  (solid curve) and  $\tau_{h2}$  (dashed curve) versus  $\mathcal{A}/\mathcal{A}_{2e}$  for a two-spike solution with  $D = 0.25$ . Right figure: Spike amplitudes for  $D = 0.25$ ,  $\varepsilon = 0.01$ , with  $\tau = 30$  (dashed curve),  $\tau = 34$  (solid curve), and  $\tau = 40$  (heavy solid curve).

### 3.4 The Infinite-Line Problem

Next, we briefly consider the stability of a one-spike equilibrium solution centered at  $x = 0$  for the infinite-line problem where (1.5) is posed on  $-\infty < x < \infty$ . The only main modification needed to the analysis leading to Principal Results 2.1 and 3.2 is that the Green's function in (2.5) must be replaced with the infinite-line Green's function  $G(x; 0)$  satisfying

$$DG_{xx} - G = -\delta(x), \quad -\infty < x < \infty; \quad G \rightarrow 0 \quad \text{as} \quad |x| \rightarrow \infty; \quad G(x; 0) = \left(\frac{\theta_0}{2}\right) e^{-\theta_0|x|}, \quad (3.43)$$

where  $\theta_0 \equiv 1/\sqrt{D}$ . Since the analysis to construct this solution parallels that in §2, we only give the result.

**Principal Result 3.16:** *Let  $\varepsilon \rightarrow 0$ , with  $\mathcal{A} = O(1)$  and  $D = O(1)$  in (1.5), defined now on  $-\infty < x < \infty$ . Then, when  $\mathcal{A} > \mathcal{A}_{1e} \equiv \sqrt{12D}^{-1/4}$ , there are two one-spike solutions given asymptotically by*

$$\nu_{\pm}(x) \sim \frac{1}{\mathcal{A}U_{\pm}} w[\varepsilon^{-1}x], \quad u_{\pm}(x) \sim 1 - \frac{6}{\mathcal{A}^2 U_{\pm}} G(x; 0), \quad U_{\pm} \equiv \frac{1}{2} \left[ 1 \pm \sqrt{1 - \frac{\mathcal{A}_{1e}^2}{\mathcal{A}^2}} \right]. \quad (3.44)$$

Here  $u_+$ ,  $\nu_+$  and  $u_-$ ,  $\nu_-$  are the small and large solutions. Also,  $w$  and  $G$  satisfy (2.2) and (3.43).

Since the derivation of the nonlocal eigenvalue problem is similar to that done in §3 for a multi-spike solution on the finite interval we again only give the main result. Consider perturbations of the form

$$\nu(x) = \nu_{\pm}(x) + e^{\lambda t} \Phi[\varepsilon^{-1}x], \quad u(x) = u_{\pm}(x) + e^{\lambda t} \eta(x). \quad (3.45)$$

Then, in terms of the local operator  $L_0$  of (3.11b), the nonlocal eigenvalue problem for  $\Phi(y)$  satisfies

$$L_0 \Phi - \chi w^2 \left( \frac{\int_{-\infty}^{\infty} w \Phi dy}{\int_{-\infty}^{\infty} w dy} \right) = \lambda \Phi, \quad -\infty < y < \infty; \quad \chi \equiv \frac{2s}{s + \sqrt{1 + \tau\lambda}}, \quad s \equiv \frac{1 - U_{\pm}}{U_{\pm}}, \quad (3.46)$$

with  $\Phi \rightarrow 0$  as  $|y| \rightarrow \infty$ . Notice that the multiplier  $\chi$  in (3.46) can be obtained by taking the limit  $D \rightarrow 0$  in the multiplier in (3.12) corresponding to a  $k$ -spike symmetric pattern on the finite line. In place of (3.16) and (3.17), we then obtain that the eigenvalues  $\lambda$  are the roots of  $g(\lambda) = 0$ , where

$$g(\lambda) \equiv C(\lambda) - f(\lambda), \quad f(\lambda) \equiv \frac{\int_{-\infty}^{\infty} w (L_0 - \lambda)^{-1} w^2 dy}{\int_{-\infty}^{\infty} w^2 dy}, \quad C(\lambda) = \frac{1}{2} + \frac{\sqrt{1 + \tau \lambda}}{2s}. \quad (3.47)$$

Although the derivation of the equilibrium solution and the nonlocal eigenvalue problem are based on formal asymptotics, the rigorous approach of §3.2 can be applied to study the spectrum of (3.46). In this way, we obtain the following result:

**Proposition 3.17:** *Let  $\varepsilon \rightarrow 0$  and consider a one-spike solution to (1.5) on the infinite line. The small solution  $u_+$ ,  $v_+$ , where  $0 < s < 1$ , is unstable for any  $\tau > 0$  as a result of a positive eigenvalue on the real axis. The large solution  $u_-$ ,  $v_-$ , where  $s > 1$ , is stable with respect to the large eigenvalues for  $\tau$  sufficiently small, and is unstable with respect to the large eigenvalues for  $\tau$  sufficiently large. There exists a value  $\tau_h = \tau_h(s)$  (possibly non-unique) where there are complex conjugate eigenvalues on the imaginary axis.*

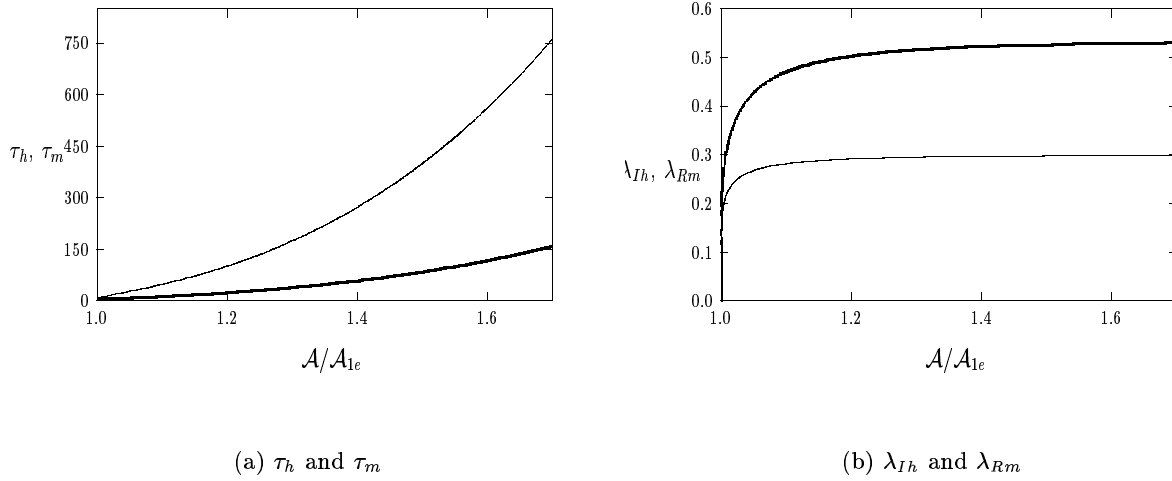


Figure 17: Left figure: the Hopf bifurcation value  $\tau_h$  (heavy solid curve) versus  $\mathcal{A}/\mathcal{A}_{1e}$ . The complex eigenvalues merge onto the positive real axis when  $\tau = \tau_m$  (solid curve). Right figure: The corresponding critical values  $\lambda_{Ih}$  (heavy solid curve) and  $\lambda_{Rm}$  (solid curve).

Using the numerical method described briefly in §3.3, we compute  $\tau_h = \tau_h(s)$  numerically. From  $s = (1 - U_{\pm})/U_{\pm}$ , we get  $\tau_h$  as a function of  $\mathcal{A}/\mathcal{A}_{1e} = (1 + s) [2\sqrt{s}]^{-1}$ . In addition, we can compute the value of  $\tau$ , labeled by  $\tau_m(s)$ , where the complex conjugate eigenvalues merge onto the real axis. A simple calculation using (3.46) together with the local properties of  $f(\lambda)$  for  $\lambda \rightarrow 0$ , as given in Propositions 3.5 and 3.7 above, shows that when  $s = 1$  there is a double root to  $g(\lambda) = 0$  at  $\lambda = 0$  and  $\tau = 3$ . The numerical results for  $\tau_h$  and  $\tau_m$  as a function of  $\mathcal{A}/\mathcal{A}_{1e}$  are shown in Fig. 17(a). Although we cannot prove that  $\tau_h$  is unique, numerical evidence suggests that when  $\tau > \tau_h$  there are always two eigenvalues in the right half-plane. In Fig. 17(b) we plot the function  $\lambda_{Ih}$  versus  $\mathcal{A}/\mathcal{A}_{1e}$  where we have a Hopf bifurcation.

In this figure we also plot the function  $\lambda_{Rm}$  versus  $\mathcal{A}/\mathcal{A}_{1e}$  where complex conjugate eigenvalues in the right half-plane first merge onto the real axis. From this figure, we notice that  $\lambda_{Ih}$  and  $\lambda_{Rm}$  have limiting behaviors for  $s \gg 1$ . This limiting behavior is analyzed in a more general context in §4. The critical value  $\tau_h$  for this infinite-line problem can be obtained by taking the limiting  $\sqrt{D}k \ll 1$  in all of the results of §3.2 for the finite domain problem (1.5). Therefore, the results for  $D = 0.1$  and  $k = 1, \dots, 3$ , computed above in §3.3, should reasonably approximate those for the infinite-line problem.

Next, we relate our results for the infinite-line problem with those of [25]. In [25] a similar formal analysis was used to construct a one-spike equilibrium solution. To show the equivalence of our nonlocal eigenvalue problem (3.46) with that in [25], we integrate (3.46) over  $-\infty < y < \infty$  to obtain

$$(2 - \chi) \int_{-\infty}^{\infty} w \Phi \, dy = (\lambda + 1) \int_{-\infty}^{\infty} \Phi \, dy. \quad (3.48)$$

Then, we solve (3.48) for  $\int_{-\infty}^{\infty} w \Phi \, dy$ . Substituting the result into (3.46), and using  $\int_{-\infty}^{\infty} w^2 \, dy = 6$ , we get

$$L_0 \Phi - \frac{\chi(\lambda + 1)}{6(2 - \chi)} w^2 \int_{-\infty}^{\infty} \Phi \, dy = \lambda \Phi. \quad (3.49)$$

For the large solution, where  $s > 1$ , we use (3.46) for  $\chi$  to write (3.49) as

$$L_0 \Phi - \frac{4\alpha}{9} w^2 \int_{-\infty}^{\infty} \Phi \, dy = \lambda \Phi, \quad \alpha \equiv \frac{3\mathcal{A}^2}{8\mathcal{A}_{1e}^2} \frac{(1 + \lambda)}{\sqrt{1 + \tau\lambda}} \left( 1 + \sqrt{1 - \frac{\mathcal{A}_{1e}^2}{\mathcal{A}^2}} \right)^2, \quad (3.50)$$

where  $w(y) = \frac{3}{2} \text{sech}^2(y/2)$ . The NLEP (3.50) is given in equation (2.13) of [25]. Our plots of  $\tau_h$  and  $\lambda_{Ih}$  are equivalent to those in Fig. 2.4c and Fig. 2.4d of [25]. In Appendix B of [25], some properties of the spectrum for (3.50) were obtained. Our rigorous approach to the nonlocal eigenvalue problem, with results summarized in Proposition 3.17, provides an alternative proof of the stability properties.

In [8] a rigorous geometric singular perturbation approach was used to establish the existence of a one-spike solution and a periodic solution to a different dimensionless form of the infinite line GS model (cf. Theorem 4.3 of [8]). For a one-spike solution, the threshold  $\mathcal{A}_{1e} = \sqrt{12}D^{-1/4}$  for the low feed-rate regime is equivalent to that in Theorem 4.3 of [8]. In [7] an alternative analysis of the NLEP (3.46) was given using dynamical systems techniques. This work is described in more detail in §4 and §5 below.

## 4 The Intermediate Regime: $O(1) \ll \mathcal{A} \ll O(\varepsilon^{-1/2})$

The derivation of the spectral problem in Principal Result 3.2 was based on linearizing (1.5) around the solution of Principal Result 2.1. A crucial feature of this solution is that the leading-order inner problems for  $u_{\pm}$  and  $\nu_{\pm}$  decouple near each spike. In particular, this implies that  $u_{\pm} = U_{\pm} + O(\varepsilon)$  in the core of each spike. The nonlocal eigenvalue problem (3.11) is valid for the range of  $\mathcal{A}$  where such a leading-order decoupling of the inner problems for  $u_{\pm}$  and  $\nu_{\pm}$  can be made. We now show formally that, when  $D = O(1)$ , this decoupling property holds for the intermediate regime  $O(1) \leq \mathcal{A} \ll O(\varepsilon^{-1/2})$ . In this regime, we then derive certain scaling laws for the stability thresholds calculated in §3.

To construct a  $k$ -spike pattern, we first construct a symmetric one-spike equilibrium solution to (1.5) on the interval  $-l < x < l$ . Then, by setting  $l = 1/k$ , we obtain the result for a  $k$ -spike solution of (1.5) on



$-1 < x < 1$ . In the inner region near  $x = 0$ , we let  $y = \varepsilon^{-1}x$ ,  $\nu_i(y) = \nu(\varepsilon y)$ ,  $u_i(y) = u(\varepsilon y)$ , and we expand the inner equilibrium solution for (1.5) on  $-l < x < l$  as

$$\nu_i(y) = \nu_{i0}(y) + \varepsilon \nu_{i1}(y) + \cdots, \quad u_i(y) = u_{i0}(y) + \varepsilon u_{i1}(y) + \cdots. \quad (4.1)$$

Substituting (4.1) into the equilibrium problem for (1.5), we collect powers of  $\varepsilon$  to get

$$\nu_{i0}'' - \nu_{i0} + \mathcal{A}u_{i0}\nu_{i0}^2 = 0; \quad u_{i0}'' = 0, \quad -\infty < y < \infty, \quad (4.2a)$$

$$\nu_{i1}'' - \nu_{i1} + 2\mathcal{A}u_{i0}\nu_{i0}\nu_{i1} = -\mathcal{A}u_{i1}\nu_{i0}^2; \quad Du_{i1}'' = u_{i0}\nu_{i0}^2, \quad -\infty < y < \infty. \quad (4.2b)$$

In terms of the solution  $w$  to (2.2), the solution to (4.2a) is simply  $\nu_{i0}(y) = w/(\mathcal{A}U)$  and  $u_{i0}(y) = U$ .

In the outer region,  $\nu$  is exponentially small and  $\varepsilon^{-1}u\nu^2$  can be represented as a Dirac mass, which can be calculated using the leading-order inner solutions  $u_{i0}$  and  $\nu_{i0}$ . Thus, the outer solution  $u_0$  satisfies

$$Du_0'' + (1 - u_0) = \frac{6}{\mathcal{A}^2 U} \delta(x) \quad -l < x < l; \quad u_{0x}(\pm l) = 0. \quad (4.3)$$

The solution to (4.3) is written in terms of the Green's function  $G_l(x, 0)$  on  $|x| < l$  satisfying

$$DG_{lxx} - G_l = -\delta(x), \quad -l < x < l; \quad G_{lx}(\pm l; 0) = 0; \quad G_l(x; 0) = \left(\frac{\theta_0}{2}\right) \frac{\cosh[(l - |x|)\theta_0]}{\sinh(l\theta_0)}, \quad (4.4)$$

where  $\theta_0 \equiv 1/\sqrt{D}$ . Then, we solve (4.3), and use the leading-order matching condition  $u_0(0) = U$  to get

$$u_0(x) = 1 - \frac{6}{\mathcal{A}^2 U} G(x; 0), \quad U = 1 - \frac{6G_l(0; 0)}{\mathcal{A}^2 U}, \quad G_l(0; 0) = \left(\frac{\theta_0}{2}\right) \coth(\theta_0 l). \quad (4.5)$$

Next, we expand  $u_0$  in one-sided limits as  $x \rightarrow 0^\pm$  to obtain the following matching condition for  $u_{i1}$ :

$$u_{i1} \sim -\frac{6G_{lx}(0^\pm; 0)}{\mathcal{A}^2 U} y, \quad \text{as } y \rightarrow \pm\infty. \quad (4.6)$$

To obtain parameter-free inner problems, we introduce new inner variables  $\hat{u}_{i1}$  and  $\hat{\nu}_{i1}$  defined by

$$u_{i1} = \frac{1}{D\mathcal{A}^2 U} \hat{u}_{i1}, \quad \nu_{i1} = \frac{1}{D\mathcal{A}^3 U^3} \hat{\nu}_{i1}. \quad (4.7)$$

Substituting (4.7) and (4.6) into (4.2), and noting that  $G_{lx}(0^\pm; 0) = \mp\theta_0^2/2$ , we obtain an explicit two-term inner expansion. The outer expansion is obtained from (4.5). Finally, by identifying  $l = 1/k$  we obtain the following formal result for a  $k$ -spike equilibrium solution:

**Principal Result 4.1:** *For  $\varepsilon \rightarrow 0$ , consider a  $k$ -spike equilibrium solution to (1.5). Then, when  $\mathcal{A} > \mathcal{A}_{ke}$  there are two such solutions; the large solution  $u_-$ ,  $\nu_-$ , and the small solution  $u_+$ ,  $\nu_+$ . The two-term inner expansions in the core of each spike are*

$$\nu_{i\pm}(y) \sim \frac{1}{\mathcal{A}U_\pm} \left[ w(y) + \frac{\varepsilon}{\mathcal{A}^2 U_\pm^2 D} \hat{\nu}_{i1}(y) + \cdots \right], \quad u_{i\pm}(y) \sim U_\pm \left[ 1 + \frac{\varepsilon}{\mathcal{A}^2 U_\pm^2 D} \hat{u}_{i1}(y) + \cdots \right], \quad (4.8a)$$

where  $U_\pm$  and  $\mathcal{A}_{ke}$  are given explicitly in (2.10). Here  $\hat{\nu}_{i1}(y)$  and  $\hat{u}_{i1}(y)$  are even solutions to the following parameter-independent inner problems on  $-\infty < y < \infty$ :

$$\hat{\nu}_{i1}'' - \hat{\nu}_{i1} + 2w\hat{\nu}_{i1} = -\hat{u}_{i1}w^2, \quad \hat{u}_{i1}'' = w^2; \quad \hat{\nu}_{i1} \rightarrow 0, \quad \hat{u}_{i1} \sim 3|y|, \quad \text{as } |y| \rightarrow \infty. \quad (4.8b)$$

In terms of the global Green's function of (2.5), the corresponding outer solution for  $u$  on  $|x| < 1$  is

$$u_0(x) = 1 - \frac{(1 - U_{\pm})}{a_g} \sum_{j=1}^k G(x; x_j), \quad a_g = \left[ 2\sqrt{D} \tanh(\theta_0/k) \right]^{-1}. \quad (4.9)$$

From (4.8a), it follows that the leading-order inner solutions can be decoupled provided that

$$\frac{\varepsilon}{\mathcal{A}^2 U_{\pm}^2 D} \ll 1. \quad (4.10)$$

Since  $U_+ \rightarrow 1$  as  $\mathcal{A} \rightarrow \infty$ , (4.10) holds uniformly as  $\mathcal{A} \rightarrow \infty$  for the small solution  $u_+$ ,  $\nu_+$ . Alternatively, as  $\mathcal{A} \rightarrow \infty$ , we have for the large solution  $u_-$ ,  $\nu_-$  that

$$U_- \sim \frac{\mathcal{A}_{ke}^2}{4\mathcal{A}^2} + O\left(\frac{\mathcal{A}_{ke}^4}{\mathcal{A}^4}\right), \quad \text{for } \mathcal{A} \gg 1. \quad (4.11)$$

Substituting (4.11) into (4.10), and using (2.10) for  $\mathcal{A}_{ke}$ , we obtain that (4.10) holds provided that

$$O(1) \leq \mathcal{A} \ll 3\varepsilon^{-1/2} \coth[\theta_0/k], \quad \theta_0 = D^{-1/2}. \quad (4.12)$$

Therefore, for  $D = O(1)$  and  $D \ll 1$ , we require that  $\mathcal{A} \ll O(\varepsilon^{-1/2})$ . Although the lower bound in (4.12) appears to hold uniformly in  $D$  as  $D \rightarrow 0$ , this is misleading because the existence threshold in (2.10) yields  $\mathcal{A}_{ke} = O(D^{-1/4})$  for  $D \ll 1$ . Hence, for  $D \ll 1$ , the intermediate regime exists provided that  $O(D^{-1/4}) \ll \mathcal{A} \ll O(\varepsilon^{-1/2})$ . This requires that  $D \gg O(\varepsilon^2)$ . Therefore, there is no intermediate range for  $\mathcal{A}$  in the weak-interaction regime  $D = O(\varepsilon^2)$  studied in [30], [31], and [38]. In this regime, the analysis of equilibrium solutions for the GS model requires a full balance of all of the terms in (1.2).

We now derive certain scaling laws in the intermediate regime  $O(1) \ll \mathcal{A} \ll O(\varepsilon^{-1/2})$  and  $D = O(1)$ . In this regime we use (4.11) to obtain the two-term inner expansion for  $u_-$  and  $\nu_-$

$$\nu_{i-}(y) \sim \frac{\mathcal{A}\sqrt{D}}{3 \coth(\theta_0/k)} [w(y) + \delta \hat{\nu}_{i1}(y) + \dots], \quad u_{i-}(y) \sim \frac{3 \coth(\theta_0/k)}{\mathcal{A}^2 \sqrt{D}} [1 + \delta \hat{u}_{i1}(y) + \dots]. \quad (4.13)$$

Here  $\delta \equiv \frac{\varepsilon \mathcal{A}^2}{9} \tanh^2(\theta_0/k) \ll 1$ . Moreover, for  $\mathcal{A} \gg 1$ , the outer solution (4.9) has the form

$$u_0(x) \sim 1 - \frac{1}{a_g} \left( 1 - \frac{\mathcal{A}_{ke}^2}{4\mathcal{A}^2} \right) \sum_{j=1}^k G(x; x_j). \quad (4.14)$$

In the intermediate regime, we can use (4.13) to calculate the norm  $|\nu|_2$  in (2.11) as

$$|\nu|_2 \equiv \left( \varepsilon^{-1} \int_{-1}^1 \nu^2 dx \right)^{1/2} \sim \frac{\sqrt{6Dk}\mathcal{A}}{3 \coth(\theta_0/k)}. \quad (4.15)$$

The expansions (4.13) and (4.14) do suggest the following scalings of the inner and outer solutions in the pulse-splitting regime  $\mathcal{A} = O(\varepsilon^{-1/2})$ , which is studied in the companion paper [17]:

$$\nu_i = O(\varepsilon^{-1/2}), \quad u_i = O(\varepsilon), \quad u_0 = u_{01} + O(\varepsilon). \quad (4.16)$$

The spectral results of §3 are valid when the decoupling condition (4.12) holds. We now derive scaling laws for the stability thresholds of the large solution in the intermediate regime. Using (4.11), we get

$$s \equiv \frac{1 - U_-}{U_-} = \frac{4\mathcal{A}^2}{\mathcal{A}_{ke}^2} - 2 + o(1), \quad \text{as } \mathcal{A} \rightarrow \infty. \quad (4.17)$$

To calculate the stability threshold  $D_{kL}$  for a competition instability, we let  $s \rightarrow \infty$  in (3.25a). From (4.17), a simple calculation shows that  $D_{kL} = O(\mathcal{A}^2)$  for  $\mathcal{A} \gg 1$ . More precisely, for  $k > 1$  we obtain

$$D_{kL} = D_{kL}^\infty + O(\mathcal{A}/\mathcal{A}_{ke}), \quad D_{kL}^\infty \equiv \frac{8\mathcal{A}^2}{k^2\gamma_k\mathcal{A}_{ke}^2} \quad \text{where } \gamma_k \equiv 1 + \cos\left(\frac{\pi}{k}\right). \quad (4.18)$$

Since  $\mathcal{A}_{ke}$  depends on  $D$ , the threshold for  $D$  can be written more explicitly by using (2.10) for  $\mathcal{A}_{ke}$  directly in (4.18). In this way, we obtain that there are no eigenvalues on the positive real axis when  $\tau$  is sufficiently small, provided that  $D < D_{kL}^\infty$ , where  $D_{kL}^\infty$  for  $k > 1$  is the unique root of

$$\sqrt{D} = \frac{2\mathcal{A}^2}{3k^2\gamma_k} \tanh\left(\frac{1}{k\sqrt{D}}\right). \quad (4.19)$$

In the intermediate regime, (4.19) can be solved asymptotically to predict a minimum inter-spike distance  $L_m$  for the stability of a spike pattern. For a  $k$ -spike pattern on a domain of length 2, the inter-spike separation is  $L = 2/k$ . For  $\mathcal{A} \gg 1$ , the root of (4.19) satisfies  $D \gg 1$ . For  $D \gg 1$ , we solve (4.19) for  $k$  with  $\mathcal{A} = \varepsilon^{-1/2}A$  to conclude that, for  $\tau$  sufficiently small, there are no positive real eigenvalues when

$$L > L_m \sim \left(\frac{12\gamma_k D \varepsilon}{A^2}\right)^{1/3}, \quad O(\varepsilon^{1/2}) \ll A \ll O(1); \quad \gamma_k = 1 + \cos(\pi/k). \quad (4.20)$$

Since  $L_m \gg O(\varepsilon)$ , the analysis leading to (4.20) is consistent. A similar scaling law was given in equation (15.58) of [15] for the minimum inter-spike separation distance of a periodic spike pattern of the Brusselator model in a particular parameter regime.

To determine the stability threshold for a Hopf bifurcation in the intermediate regime, we let  $s \rightarrow \infty$  in (3.17) to get  $C_j = (1/2) + O(s^{-1})$  for  $\tau = O(1)$  and  $D = O(1)$ . Since  $C_j \sim 1/2$ , there are no eigenvalues in the right half-plane (cf. Appendix E of [14] and Theorem 1.4 of [40]). Thus, for  $D = O(1)$ , an instability can only occur when  $\tau \gg 1$ . The correct scaling law is to introduce a new  $O(1)$  parameter  $\tau_0$  by

$$\tau = \tau_0 \tanh^2(\theta_0/k) s^2. \quad (4.21)$$

Substituting (4.21) into (3.17), and assuming that  $D = O(1)$ , we let  $s \rightarrow \infty$  to obtain

$$C_j(\lambda) \sim C_\infty(\lambda) + O(s^{-2}), \quad C_\infty(\lambda) \equiv \frac{1}{2} \left[1 + \sqrt{\tau_0 \lambda}\right]. \quad (4.22)$$

Notice that  $C_\infty(\lambda)$  is independent of  $j$ , of  $D$ , and of the number of spikes  $k$ . The nonlocal eigenvalue problem in the intermediate regime is then obtained by replacing  $\chi$  in (3.11) with  $\chi = 1/C_\infty$ . Substituting (4.17) into (4.21), we obtain the key scaling law

$$\tau \sim \tau_\infty \equiv \frac{16\mathcal{A}^4}{\mathcal{A}_{ke}^4} \tanh^2(\theta_0/k) \tau_0 \left(1 - \frac{\mathcal{A}_{ke}^2}{2\mathcal{A}^2}\right)^2 + o(1). \quad (4.23)$$

Formally this leads to the following nonlocal eigenvalue problem in the intermediate regime:

**Principal Result 4.2:** *Assume that  $0 < \varepsilon \ll 1$ ,  $D = O(1)$ , and  $O(1) \ll \mathcal{A} \ll O(\varepsilon^{-1/2})$ . Then, with  $\Phi = \Phi(y)$ , the  $O(1)$  eigenvalues of (2.14) for a symmetric  $k$ -spike large solution  $u_-$ ,  $\nu_-$  satisfy, for each  $j = 1, \dots, k$ , the following universal nonlocal eigenvalue problem:*

$$L_0 \Phi - \chi_\infty w^2 \left( \frac{\int_{-\infty}^{\infty} w \Phi dy}{\int_{-\infty}^{\infty} w dy} \right) = \lambda \Phi, \quad -\infty < y < \infty; \quad \chi_\infty \equiv \frac{2}{1 + \sqrt{\tau_0 \lambda}}, \quad (4.24)$$

with  $\Phi \rightarrow 0$  as  $|y| \rightarrow \infty$ . In (4.24) the local operator  $L_0$  is given in (3.11b). The corresponding global eigenfunction  $\phi(x)$ , representing the perturbation in  $\nu_-$ , satisfies  $\phi(x) \sim \sum_{i=1}^k c_i \Phi[\varepsilon^{-1}(x - x_i)]$ . Here  $c_i$  for  $i = 1, \dots, k$  are the components of any one of the  $k$  independent eigenvectors in (3.10b).

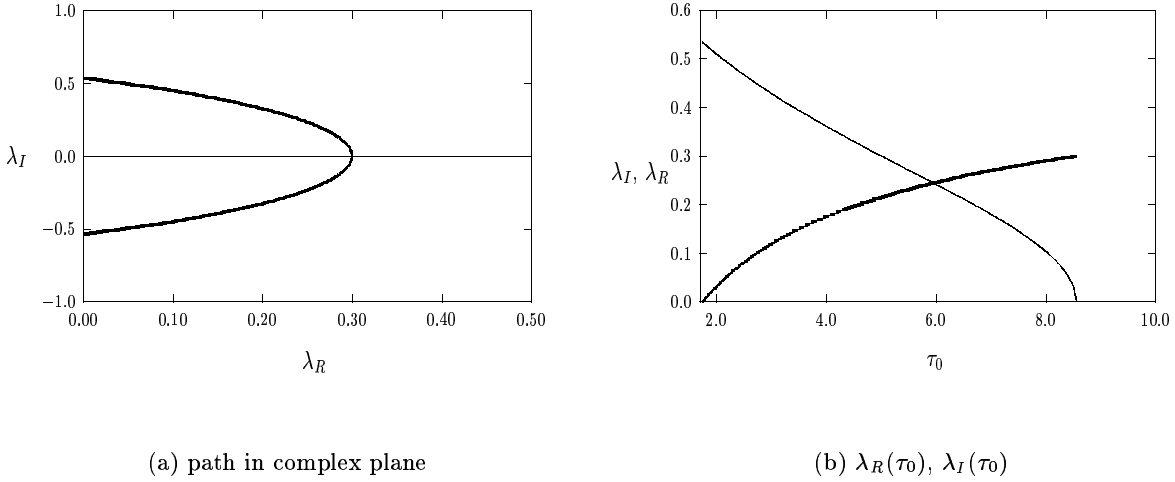


Figure 18: Left figure: plot of the path of  $\lambda = \lambda_R \pm i\lambda_I$  as  $\tau_0$  increases past  $\tau_{0h} = 1.748$  until it merges onto the real axis at  $\tau_{0m} = 8.567$ . Right figure:  $\lambda_R$  (heavy solid curve) and  $\lambda_I$  (solid curve) versus  $\tau_0$ .

In terms of a different dimensionless form of the GS model (1.2), the eigenvalue problem (4.24) was also derived and studied in [6] and [7] using a dynamical systems approach. In [6] and [7], hypergeometric functions were used to numerically compute a winding number criterion for (4.24) over a wedge-shaped region that includes part of the left half-plane. Since the continuous spectrum is on the negative real axis, there were many technical difficulties that were overcome with the approach in [7] in order to count the number of eigenvalues near the origin. In our analysis of §3, by having derived properties of  $f(\lambda)$  on the imaginary axis, we do not need to consider the left half-plane and the difficulties with the continuous spectrum intersecting the origin. The only effect of the continuous spectrum with our formulation is that  $C'_\infty(0)$  is infinite. Even with this change in the property of  $C$  in Proposition 3.6, the theory of §3 applies directly to (4.24), and proves that there is a Hopf bifurcation value  $\tau_{0h}$  (possibly non-unique) where (4.24) has complex conjugate eigenvalues on the imaginary axis. In addition, the theory of §3 also readily proves that there is another critical value  $\tau_{0m}$  where unstable complex conjugate eigenvalues first merge onto the positive real axis at some  $\lambda_{Rm}$  as  $\tau_0$  is increased.

For increasing values of  $\tau_0$ , in Fig. 18(a) we plot the numerically computed path of the unstable eigenvalues for (4.24) up until they merge onto the real axis. The corresponding functions  $\lambda_R = \lambda_R(\tau)$  and  $\lambda_I = \lambda_I(\tau) > 0$  are shown in Fig. 18(b). These numerical results suggest the stronger statement that  $\tau_{0h}$  is in fact unique, and that there are always two eigenvalues of (4.24) in the right half-plane when  $\tau_0 > \tau_{0h}$ . Our computations yield the critical values,

$$\tau_{0h} = 1.748, \quad \lambda_{Ih} = 0.534; \quad \tau_{0m} = 8.567, \quad \lambda_{Rm} = 0.300. \quad (4.25)$$

As shown in §5, these values are consistent with those in [6]. To obtain our scaling laws, we substitute (2.10) for  $\mathcal{A}_{ke}$  into (4.23). In this way, and in analogy with Proposition 3.15, we can then summarize our stability results for the large solution in the intermediate regime.

**Proposition 4.3:** *Let  $\varepsilon \ll 1$ , and consider the intermediate regime  $O(1) \ll \mathcal{A} \ll O(\varepsilon^{-1/2})$  for a symmetric  $k$ -spike large solution  $u_-, \nu_-$ . Then, when  $D = O(1)$ , the solution is stable with respect to the large eigenvalues when  $\tau < \tau_h^\infty$ , where*

$$\tau_h^\infty \sim \frac{\mathcal{A}^4 D}{9} \tanh^4(\theta_0/k) \tau_{0h} \left( 1 - \frac{6\theta_0}{\mathcal{A}^2 \tanh(\theta_0/k)} \right)^2 + o(1). \quad (4.26)$$

Moreover, for  $D = O(1)$ , two unstable complex conjugate eigenvalues merge onto the positive real axis in the interval  $0 < \lambda < 5/4$  when  $\tau = \tau_m^\infty$ , where  $\tau_m^\infty \sim \tau_h^\infty \tau_{0m}/\tau_{0h}$ . The numerically computed values are  $\tau_{0h} = 1.748$  and  $\tau_{0m} = 8.567$ . Next, suppose that  $D > D_{kL}^\infty$ , where  $D_{kL}^\infty \gg 1$  is given in (4.18). Then, the large is unstable for any  $\tau > 0$ .

As shown in §5, the leading term in the scaling law for  $\tau_h^\infty$  and  $\tau_m^\infty$  agrees with previous results in [6]. The extra term in the brackets in (4.26) is a new correction term. In contrast to the NLEP (3.11) of the low feed-rate regime, where there are  $k$  different multipliers  $\chi$ , the key feature of the NLEP problem (4.24) of the intermediate regime is that a  $k$ -spike solution is associated with exactly one multiplier  $\chi$ . This suggests a certain complexity in the dynamics near the Hopf bifurcation point, since there are  $k$  possible eigenfunctions in Principal Result 4.2 that occur when  $\tau$  crosses past  $\tau_h^\infty$ . Therefore, in contrast to the low feed-rate regime, there is no apriori guarantee that spike oscillations will be synchronous in the intermediate regime. This complexity in the dynamics was observed numerically in [6], without any theoretical explanation, where it was noted that the behavior near the Hopf bifurcation point is quite unpredictable and sensitive to perturbations (see page 30 of [6]).

In Fig. 19(a) and Fig. 19(b) we compare the scaling law (4.26) for  $\tau_h^\infty$  with the corresponding numerical value computed from (3.11) for  $k = 1$  and  $k = 2$ , respectively. From these figures, we observe that  $\tau_h^\infty$  provides a good approximation to the numerically computed value except near the existence threshold  $\mathcal{A}_{ke}$ . We remark that the leading-order approximation to  $\tau_h^\infty$ , obtained by neglecting the correction term in the bracket in (4.26), is in only fair agreement with the numerical stability threshold.

Finally, we remark that a similar scaling law for a Hopf bifurcation can be derived for the infinite-line problem of §3.4. Letting  $s \rightarrow \infty$  in (3.46), we obtain that the Hopf bifurcation value  $\tau_h^\infty$  is given by

$$\tau_h^\infty \sim \frac{\mathcal{A}^4 D}{9} \tau_{0h} \left( 1 - \frac{6\theta_0}{\mathcal{A}^2} \right)^2 + o(1), \quad (4.27)$$

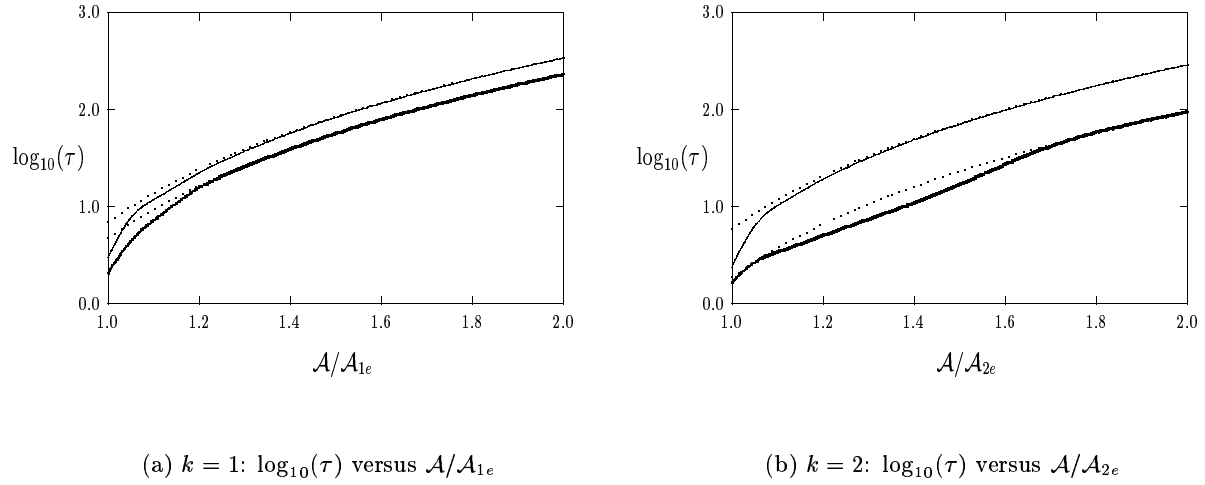


Figure 19: Comparison of numerical Hopf bifurcation value  $\log_{10}(\tau_{hL})$  (solid curve is  $D = 0.1$ , heavy solid curve is  $D = 0.75$ ) with the asymptotic scaling law  $\log_{10}(\tau_h^\infty)$ , where  $\tau_h^\infty$  is given in (4.26) (dashed curves). Left figure:  $k = 1$ . Right figure:  $k = 2$ .

where  $\theta_0 = 1/\sqrt{D}$ . Here  $\tau_{0h}$ , computed from (4.24), is given in (4.25). If we set  $D = 1$ , and write  $A = \varepsilon^{1/2}\mathcal{A}$ , then the following leading term in (4.27) is equivalent to equation (2.11) of [25]:

$$\tau_h^\infty \sim 0.19422A^4\varepsilon^{-2}. \quad (4.28)$$

## 5 Discussion and Comparisons

In this section we discuss more precisely the relationship between our results and those in the literature. We also list some open problems.

In §3.2 and in §4 we compared our results with those of [25], which were based on the infinite-line problem in both the low feed-rate and intermediate regimes. Our results in those regimes are completely consistent with those of [25].

Next, we compare our results with those of [6] and [7] for the GS model with nondimensional form

$$V_T = \delta^2 V_{XX} - \delta^\beta bV + UV^2, \quad 0 < X < L, \quad T > 0; \quad V_X = 0, \quad X = 0, L, \quad (5.1a)$$

$$U_T = U_{XX} + \delta^2 a(1 - U) - UV^2, \quad 0 < X < L, \quad T > 0; \quad U_X = 0, \quad X = 0, L. \quad (5.1b)$$

Here  $0 < \beta < 1$ , and  $\delta \ll 1$ . In [6], solutions of a spatial period  $\mathcal{T}$  are constructed formally. For a  $k$ -spike solution, this determines  $L$  as  $L = \mathcal{T}k$ . In terms of our dimensionless groupings of (1.2), it follows that

$$D \equiv \frac{4}{\delta^2 a \mathcal{T}^2 k^2}, \quad \varepsilon^2 \equiv \frac{4\delta^{2-\beta}}{b \mathcal{T}^2 k^2}, \quad \tau \equiv \frac{\delta^{\beta-2} b}{a}, \quad A \equiv \frac{\delta^{1-\beta} \sqrt{a}}{b}. \quad (5.2)$$

In equation (2.10) of [6], the mode  $m$  of the periodic pattern is related to the period  $\mathcal{T}$  by

$$m = \frac{E^2 + 1}{E^2 - 1} = \frac{1}{\tanh(\log E)}, \quad E \equiv e^{\mathcal{T}\delta\sqrt{a}/2}. \quad (5.3)$$

Using  $L = \mathcal{T}k$  and (5.2), we can express  $m$  in terms of our notation as

$$m = [\tanh(\theta_0/k)]^{-1}, \quad \theta_0 \equiv D^{-1/2}. \quad (5.4)$$

The only nonlocal eigenvalue problem studied in [6] and [7] is given in equation (4.14) of [6]. Using (5.2), it is readily shown that equation (4.14) of [6] is exactly equivalent to the intermediate regime NLEP (4.24) of Principal Result 4.2. In [6], hypergeometric functions were used to study this NLEP. In this way, it was shown in equation (5.16) of [6] that there is a Hopf bifurcation at  $b = b_h$  and that a pair of unstable complex conjugate eigenvalues merge onto the positive real axis at  $b = b_c$ . These critical values were

$$b = b_h \equiv \frac{\sqrt{a}}{m} \delta^{1/2-\beta} (0.66), \quad b = b_c \equiv \frac{\sqrt{a}}{m} \delta^{1/2-\beta} (0.99). \quad (5.5)$$

We now show that these results agree precisely with the leading-order terms for the scaling-laws  $\tau_h^\infty$  and  $\tau_m^\infty$  given in Proposition 4.3. To show this, we write the leading term in (4.26) as

$$\tau_h^\infty \sim \frac{\mathcal{A}^4 D}{9} \tanh^4(\theta_0/k) \tau_{0h} = \frac{\varepsilon^{-2} A^4 D}{9} \tanh^4(\theta_0/k) \tau_{0h}. \quad (5.6)$$

Using the change of variables (5.2), which relates our notation to that of [6], we obtain

$$\frac{\delta^{\beta-2} b}{a} = \frac{\delta^{-3\beta} a}{b^3} \tanh^4(\theta_0/k) \left( \frac{\tau_{0h}}{9} \right). \quad (5.7)$$

Solving (5.7) for  $b$ , and recalling (5.4) for  $m$ , we obtain

$$b = \frac{\sqrt{a}}{m} \delta^{1/2-\beta} \left( \frac{\tau_{0h}}{9} \right)^{1/4}. \quad (5.8)$$

Recalling from (4.25) that  $\tau_{0h} = 1.748$ , we observe that (5.8) and (5.5) agree. Similarly, the leading-order term for  $\tau_m^\infty$  in Proposition 4.3 agrees with  $b_c$  in (5.5).

Therefore, our results for the stability of  $k$ -spike patterns in the intermediate regime agree asymptotically with those of [6]. However, there are a few differences in the approach and in the results. Firstly, our rigorous analysis of the nonlocal eigenvalue problem in Principal Result 4.2 provides a simple alternative proof to the study in [6] and [7], which uses dynamical systems techniques and computations involving hypergeometric functions to establish the existence of a Hopf bifurcation point. Secondly, the scaling laws in Proposition 4.3 incorporate an extra correction term not given in [6] (see Fig. 19). Without this term, only fair agreement is obtained with numerically computed Hopf bifurcation thresholds. Finally, we have provided a new scaling law in (4.20) for competition instabilities of closely spaced spikes.

However, the essential difference between our study and that of previous studies is our analysis of the low-feed rate regime in §2 and §3. The eigenvalue problem of Principal Result 3.2 is new in the context of the GS model. It leads to the existence of both competition and (typically) synchronous oscillatory instabilities. These instabilities have not been reported previously for the GS model. In addition, Proposition 3.3 shows a clear equivalence between the GS and GM models in the low feed-rate regime. In the intermediate regime, the stability analysis of  $k$ -spike patterns is essentially very simple, in that the scaling laws described above show that the stability threshold for a  $k$ -spike pattern is a multiple of the threshold for a one-spike pattern.

This simplification does not occur for the GS model in the low-feed rate regime, and consequently the stability analysis there is much more intricate than in the intermediate regime.

There are several open problems related to this study. Regarding large-scale behavior away from bifurcation points, an open problem is to analyze the large-scale synchronous oscillatory instabilities and competition instabilities that occur in the low feed-rate regime after they are initiated. In this context, it is an open problem to prove that the oscillatory instability in the GS model is subcritical. The oscillatory instabilities in the GM model studied in [39] often lead to stable large-scale time-periodic solutions. It would be interesting to calculate the normal form of these oscillations for both the GS and GM models to show the differences in the behavior of the oscillations. A key technical problem, for both the low feed-rate and intermediate regimes, is to prove a strict transversal crossing condition to guarantee that the complex conjugate eigenvalues on the imaginary axis when  $\tau = \tau_{hL}$  remain in the right half-plane for any  $\tau > \tau_{hL}$ . Numerical evidence suggests that this is the case, but an analytical proof is not available. Another open problem is to determine if there is a wide parameter regime where asynchronous oscillations in the spike amplitudes are possible. It would also be interesting to characterize the dynamics of quasi-equilibrium patterns in the low and intermediate feed-rate regimes. For the GM model (1.7), such an analysis of the dynamics of quasi-equilibrium patterns was done for a  $k$ -spike pattern with  $\tau = 0$  in [12], and for a one-spike pattern with  $\tau > 0$  in [36]. Two-spike evolutions were analyzed in [4] and [5] on the infinite line, and in [37] on a finite domain. Finally, since our analysis does not rely on dynamical systems techniques, much of it is readily extended to treat the stability and dynamics of two-dimensional spot patterns for the GS model. Work in this direction is in progress.

## Acknowledgements

T. K. was supported by a PGS-B graduate scholarship from NSERC (Canada). M. J. W. thanks the grant support of NSERC, the hospitality of the IMS of the Chinese University of Hong Kong, and the generous use of computer facilities from the University of Washington Applied Math group. J. W. thanks the support of RGC of Hong Kong and a direct grant from CUHK. We would also like to thank an anonymous referee for his careful reading of the paper, and for his comments on spatial scaling laws for competition instabilities.

## References

- [1] U. Ascher, R. Christiansen, R. Russell, *Collocation Software for Boundary Value ODE's*, Math. Comp., **33**, (1979), pp. 659–679.
- [2] A. Bose, G. Kriegsmann, *Stability of Localized Structures in NonLocal Reaction-Diffusion Equations*, Meth. Appl. Anal., **5**, No. 4, (1998), pp. 351–366.
- [3] A. Bose, *A Geometric Approach to Singularly Perturbed Nonlocal Reaction Diffusion Equations*, SIAM J. Math. Anal., **31**, No. 2, (2000), pp. 431–454.
- [4] A. Doelman, W. Eckhaus, T. J. Kaper, *Slowly Modulated Two-Pulse Solutions in the Gray-Scott Model I: Asymptotic Construction and Stability*, SIAM J. Appl. Math., **61**, No. 3, (2000), pp. 1080–1102.



- [5] A. Doelman, W. Eckhaus, T. J. Kaper, *Slowly Modulated Two-Pulse Solutions in the Gray-Scott Model II: Geometric Theory, Bifurcations, and Splitting Dynamics*, SIAM J. Appl. Math., **61**, No. 6, (2000), pp. 2036–2061.
- [6] A. Doelman, R. A. Gardner, T. J. Kaper, *Stability Analysis of Singular Patterns in the 1D Gray-Scott Model: A Matched Asymptotics Approach*, Physica D, **122**, No. 1-4, (1998), pp. 1–36.
- [7] A. Doelman, R. A. Gardner, T. Kaper, *A Stability Index Analysis of 1-D Patterns of the Gray Scott Model*, Memoirs of the AMS, **155**, No. 737, (2002).
- [8] A. Doelman, T. J. Kaper, P. Zegeling, *Pattern Formation in the One-Dimensional Gray-Scott Model*, Nonlinearity, **10**, No. 2, (1997), pp. 523–563.
- [9] A. Gierer, H. Meinhardt, *A Theory of Biological Pattern Formation*, Kybernetik, **12**, (1972), pp. 30–39.
- [10] P. Gray, S. K. Scott, *Autocatalytic Reactions in the Isothermal, Continuous Stirred Tank Reactor: Oscillations and Instabilities in the System  $A + 2B \rightarrow 3B$ ,  $B \rightarrow C$* , Chem. Eng. Sci. **39**, (1984), pp. 1087–1097.
- [11] L. Harrison, D. Holloway, *Order and Localization in Reaction-Diffusion Pattern*, Physica A, **222**, (1995), pp. 210–233.
- [12] D. Iron, M. J. Ward, *The Dynamics of Multi-Spike Solutions to the One-Dimensional Gierer-Meinhardt Model*, SIAM J. Appl. Math., **62**, No. 6, (2002), pp. 1924–1951.
- [13] D. Iron, M. J. Ward, *The Stability and Dynamics of Hot-Spot Solutions for a One-Dimensional Microwave Heating Model*, Analysis and Applications, Vol. 2, No. 1, (2004), pp. 21–70.
- [14] D. Iron, M. J. Ward, J. Wei, *The Stability of Spike Solutions to the One-Dimensional Gierer-Meinhardt Model*, Physica D, **150**, No. 1-2, (2001), pp. 25–62.
- [15] B. S. Kerner, V. V. Osipov, *Autosolitons: A New Approach to Problem of Self-Organization and Turbulence*, Kluwer Academic Publishers, Dordrecht, (1994).
- [16] B. S. Kerner, V. V. Osipov, *On the Spontaneous Onset of Irregular or Pulsating Structures at the Stratification of the Uniform State of Nonequilibrium Systems*, Sov. Phys., Doklady, **28**, No. 6, (1983), pp. 485–487.
- [17] T. Kolokolnikov, M. Ward, J. Wei, *The Existence and Stability of Spike Equilibria in the One-Dimensional Gray-Scott Model: The Pulse-Splitting Regime*, submitted, Physica D., (2003).
- [18] T. Kolokolnikov, M. Ward, J. Wei, *Slow Translational Instabilities of Spike Patterns in the One-Dimensional Gray-Scott Model*, submitted, Disc. Cont. Dynam. Sys. Series B, (2005).
- [19] K. J. Lee, W. D. McCormick, J. E. Pearson, H. L. Swinney, *Experimental Observation of Self-Replicating Spots in a Reaction-Diffusion System*, Nature, **369**, (1994), pp. 215–218.
- [20] K. J. Lee, H. L. Swinney, *Lamellar Structures and Self-Replicating Spots in a Reaction-Diffusion System*, Phys. Rev. E., **51**, (1995), pp. 1899–1915.
- [21] C. S. Lin, W. M. Ni, I. Takagi, *Large Amplitude Stationary Solutions to a Chemotaxis System*, J. Diff. Eq., **72**, (1988), pp. 1–27.
- [22] H. Meinhardt, *Models of Biological Pattern Formation*, Academic Press, London, (1982).
- [23] H. Meinhardt, *The Algorithmic Beauty of Sea Shells*, Springer-Verlag, Berlin, (1995).

- [24] C. Muratov, V. V. Osipov, *Traveling Spike Auto-Solitons in the Gray-Scott Model*, Physica D, **155**, No. 1-2, (2001), pp. 112–131.
- [25] C. Muratov, V. V. Osipov, *Stability of the Static Spike Autosolitons in the Gray-Scott Model*, SIAM J. Appl. Math., **62**, No. 5, (2002), pp. 1463–1487.
- [26] C. Muratov, V. V. Osipov, *Static Spike Autosolitons in the Gray-Scott Model*, J. Phys. A: Math Gen. **33**, (2000), pp. 8893–8916.
- [27] NAG Fortran library Mark 17, routine D03PCF, Numerical Algorithms Group Ltd., Oxford, United Kingdom (1995).
- [28] Y. Nishiura, *Global Bifurcational Approach to the Onset of Spatio-Temporal Chaos in Reaction-Diffusion Systems*, Methods and Appl. of Analysis, **8**, No. 2, (2001), pp. 321–332.
- [29] Y. Nishiura, *Coexistence of Infinitely Many Stable Solutions to Reaction-Diffusion Equations in the Singular Limit*, in Dynamics Reported: Expositions in Dynamical Systems Volume 3 (editors: C. K. R. T. Jones, U. Kirchgraber), Springer-Verlag, New York, (1995).
- [30] Y. Nishiura, D. Ueyama, *A Skeleton Structure of Self-Replicating Dynamics*, Physica D, **130**, No. 1-2, (1999), pp. 73–104.
- [31] Y. Nishiura, D. Ueyama, *Spatio-Temporal Chaos for the Gray-Scott Model*, Physica D, **150**, No. 3-4, (2001), pp. 137–162.
- [32] J. E. Pearson, *Complex Patterns in a Simple System*, Science, **216**, (1993), pp. 189–192.
- [33] V. Petrov, S. K. Scott, K. Showalter, *Excitability, Wave Reflection, and Wave Splitting in a Cubic Autocatalysis Reaction-Diffusion System*, Phil. Trans. Roy. Soc. London, Series A, **347**, (1994), pp. 631–642.
- [34] W. N. Reynolds, S. Ponce-Dawson, J. E. Pearson, *Dynamics of Self-Replicating Patterns in Reaction-Diffusion Systems*, Phys. Rev. Lett., **72**, (1994), pp. 2797–2800.
- [35] W. N. Reynolds, S. Ponce-Dawson, J. E. Pearson, *Dynamics of Self-Replicating Spots in Reaction-Diffusion Systems*, Phys. Rev. E, **56**, No. 1, (1997), pp. 185–198.
- [36] W. Sun, T. Tang, M. J. Ward, J. Wei, *Numerical Challenges for Resolving Spike Dynamics for Two Reaction-Diffusion Systems*, Studies in Appl. Math., **111**, (2003), pp. 41–84.
- [37] W. Sun, M. J. Ward, R. Russell, *The Slow Dynamics of Two-Spike Solutions for the Gray-Scott and Gierer-Meinhardt Systems: Competition and Oscillatory Instabilities*, submitted, SIAM J. App. Dyn. Systems, April (2004).
- [38] D. Ueyama, *Dynamics of Self-Replicating Patterns in the One-Dimensional Gray-Scott Model*, Hokkaido Math J., **28**, No. 1, (1999), pp. 175–210.
- [39] M. J. Ward, J. Wei, *Hopf Bifurcations and Oscillatory Instabilities of Spike Solutions for the One-Dimensional Gierer-Meinhardt Model*, Journal of Nonlinear Science, **13**, No. 2, (2003), pp. 209–264.
- [40] J. Wei, *On Single Interior Spike Solutions for the Gierer-Meinhardt System: Uniqueness and Stability Estimates*, Europ. J. Appl. Math., **10**, No. 4, (1999), pp. 353–378.
- [41] J. Wei, M. Winter, *Existence and Stability Analysis of Asymmetric Patterns for the Gierer-Meinhardt System*, J. Math. Pures Appl. (9), **83**, No. 4, (2004), pp. 433–476.